Time-dependent Density Functional Theory

Miguel A. L. Marques and E. K. U. Gross

1 Introduction

Time-dependent density-functional theory (TDDFT) extends the basic ideas of ground-state density-functional theory (DFT) to the treatment of excitations or more general time-dependent phenomena. TDDFT can be viewed an alternative formulation of time-dependent quantum mechanics but, in contrast to the normal approach that relies on wave-functions and on the many-body Schrödinger equation, its basic variable is the one-body electron density, $n(\boldsymbol{r}, t)$. The advantages are clear: The many-body wave-function, a function in a $3N$-dimensional space (where N is the number of electrons in the system), is a very complex mathematical object, while the density is a simple function that depends solely on 3 variables, x, y and z. The standard way to obtain $n(\boldsymbol{r}, t)$ is with the help of a fictitious system of non-interacting electrons, the Kohn-Sham system. The final equations are simple to tackle numerically, and are routinely solved for systems with a large number of atoms. These electrons feel an effective potential, the time-dependent Kohn-Sham potential. The exact form of this potential is unknown, and has therefore to be approximated.

The scheme is perfectly general, and can be applied to essentially any time-dependent situation. Two regimes can however be observed: If the time-dependent potential is weak, it is sufficient to resort to linear-response theory to study the system. In this way it is possible to calculate, e.g. optical absorption spectra. It turns out that, even with the simplest approximation to the Kohn-Sham potential, spectra calculated within this framework are in very good agreement with experimental results. On the other hand, if the time-dependent potential is strong, a full solution of the Kohn-Sham equations is required. A canonical example of this regime is the treatment of atoms or molecules in strong laser fields. In this case, TDDFT is able to describe non-linear phenomena like high-harmonic generation, or multi-photon ionization.

Our purpose, while writing this chapter, is to provide a pedagogical introduction to TDDFT[1]. With that in mind, we present, in section 2, a quite detailed proof of the Runge-Gross theorem[5], i.e. the time-dependent generalization of the Hohenberg-Kohn theorem[6], and the corresponding

[1] The reader interested in a more technical discussion is therefore invited to read Ref. [1–4], where also very complete and updated lists of references can be found.

Kohn-Sham construction[7]. These constitute the mathematical foundations of TDDFT. Several approximate exchange-correlation (xc) functionals are then reviewed. In section 3 we are concerned with linear-response theory, and with its main ingredient, the xc kernel. The calculation of excitation energies is treated in the following section. After giving a brief overlook of the competing density-functional methods to calculate excitations, we present some results obtained from the full solution of the Kohn-Sham scheme, and from linear-response theory. Section 5 is devoted to the problem of atoms and molecules in strong laser fields. Both high-harmonic generation and ionization are discussed. Finally, the last section is reserved to some concluding remarks.

For simplicity, we will write all formulae for spin-saturated systems. Obviously, spin can be easily included in all expressions when necessary. Hartree atomic units ($e = \hbar = m = 1$) will be used throughout this chapter.

2 Time-dependent DFT

2.1 Preliminaries

A system of N electrons with coordinates $\underline{\boldsymbol{r}} = (\boldsymbol{r}_1 \cdots \boldsymbol{r}_N)$ is known to obey the time-dependent Schrödinger equation

$$\mathrm{i}\frac{\partial}{\partial t}\Psi(\underline{\boldsymbol{r}}, t) = \hat{H}(\underline{\boldsymbol{r}}, t)\Psi(\underline{\boldsymbol{r}}, t)\,, \tag{1}$$

This equation expresses one of the most fundamental postulates of quantum mechanics, and is one of the most remarkable discoveries of physics during the XXth century. The absolute square of the electronic wave-function, $|\Psi(\underline{\boldsymbol{r}}, t)|^2$, is interpreted as the probability of finding the electrons in positions $\underline{\boldsymbol{r}}$. The Hamiltonian can be written in the form

$$\hat{T}(\underline{\boldsymbol{r}}) + \hat{W}(\underline{\boldsymbol{r}}) + \hat{V}_{\mathrm{ext}}(\underline{\boldsymbol{r}}, t)\,. \tag{2}$$

The first term is the kinetic energy of the electrons

$$\hat{T}(\underline{\boldsymbol{r}}) = -\frac{1}{2}\sum_{i=1}^{N}\nabla_i^2\,, \tag{3}$$

while $\hat{W}$ accounts for the Coulomb repulsion between the electrons

$$\hat{W}(\underline{\boldsymbol{r}}) = \frac{1}{2}\sum_{\substack{i,j=1\\ i\neq j}}^{N}\frac{1}{|\boldsymbol{r}_i - \boldsymbol{r}_j|}\,. \tag{4}$$

Furthermore, the electrons are under the influence of a generic, time-dependent potential, $\hat{V}_{\mathrm{ext}}(\underline{\boldsymbol{r}}, t)$. The Hamiltonian (2) is completely general and describes

a wealth of physical and chemical situations, including atoms, molecules, and solids, in arbitrary time-dependent electric or magnetic fields, scattering experiments, etc. In most of the situations dealt with in this article we will be concerned with the interaction between a laser and matter. In that case, we can write the time-dependent potential as the sum of the nuclear potential and a laser field, $\hat{V}_{\rm TD} = \hat{U}_{\rm en} + \hat{V}_{\rm laser}$. The term $\hat{U}_{\rm en}$ accounts for the Coulomb attraction between the electrons and the nuclei,

$$\hat{U}_{\rm en}(\underline{\boldsymbol{r}}, t) = -\sum_{\nu=1}^{N_{\rm n}} \sum_{i=1}^{N} \frac{Z_\nu}{|\boldsymbol{r}_i - \boldsymbol{R}_\nu(t)|}\,, \tag{5}$$

where Z_ν and $\boldsymbol{R}_\nu$ denote the charge and position of the nucleus ν, and $N_{\rm n}$ stands for the total number of nuclei in the system. Note that by allowing the $\boldsymbol{R}_\nu$ to depend on time we can treat situations where the nuclei move along a classical path. This may be useful when studying, e.g., scattering experiments, chemical reactions, etc. The laser field, $\hat{V}_{\rm laser}$, reads, in the length gauge,

$$\hat{V}_{\rm laser}(\underline{\boldsymbol{r}}, t) = E\, f(t)\, \sin(\omega t) \sum_{i=1}^{N} \boldsymbol{r}_i \cdot \boldsymbol{\alpha}\,, \tag{6}$$

where $\boldsymbol{\alpha}$, ω and E are respectively the polarization, the frequency and the amplitude of the laser. The function $f(t)$ is a envelope that shapes the laser pulse during time. Note that in writing Eq. (6) we use two approximations: i) We treat the laser field classically, i.e., we do not quantize the photon field. This is a well justified procedure when the density of photons is large and the individual (quantum) nature of the photons can be disregarded. In all cases presented in this article this will be the case. ii) Expression (6) is written within the dipole approximation. The dipole approximation holds whenever (a) The wave-length of the light ($\lambda = 2\pi c/\omega$, where c is the velocity of light in vacuum) is much larger than the size of the system. This is certainly true for all atoms and most molecules we are interested in. However, one has to be careful when dealing with very large molecules (e.g. proteins) or solids. (b) The path that the particle travels in one period of the laser field is small compared to the wavelength. This implies that the average velocity of the electrons, v, fulfills $vT \ll \lambda \Rightarrow v \ll \lambda/T = c$, where T stands for the period of the laser. In these circumstances we can treat the laser field as a purely electric field and completely neglect its magnetic component. This approximation holds if the intensity of the laser is not strong enough to accelerate the electrons to relativistic velocities. (c) The total duration of the laser pulse should be short enough so that the molecule does not leave the focus of the laser during the time the interaction lasts.

Although the many-body Schrödinger equation, Eq. (1), achieves, to our best knowledge, a remarkably good description of nature, it poses a tantalizing problem to scientists. Its exact (in fact, numerical) solution has been achieved so far for a disappointingly small number of particles. In fact, even

the calculation of a "simple" two electron system (the Helium atom) in a laser field takes several months in a modern computer[8] (see also the work on the H_2^+[9] molecule and the H_3^{++} molecule[10]). The effort to solve Eq. (1) grows exponentially with the number of particles, therefore rapid developments regarding the exact solution of the Schrödinger equation are not expected.

In these circumstances, the natural approach of the theorist is to transform and approximate the basic equations to a manageable level that still retains the qualitative and (hopefully) quantitative information about the system. Several techniques have been developed throughout the years in the quantum chemistry and physics world. One such technique is TDDFT. Its goal, like always in density-functional theories, is to replace the solution of the complicated many-body Schrödinger equation by the solution of the much simpler one-body Kohn-Sham equations, thereby relieving the computational burden.

The first step of any DFT is the proof of a Hohenberg-Kohn type theorem[6]. In its traditional form, this theorem demonstrates that there exists a one-to-one correspondence between the external potential and the (one-body) density. With the external potential it is always possible (in principle) to solve the many-body Schrödinger equation to obtain the many-body wave-function. From the wave-function we can trivially obtain the density. The second implication, i.e. that the knowledge of the density is sufficient to obtain the external potential, is much harder to prove. In their seminal paper, Hohenberg and Kohn used the variational principle to obtain a proof by *reductio ad absurdum*. Unfortunately, their method cannot be easily generalized to arbitrary DFTs. The Hohenberg-Kohn theorem is a very strong statement: From the density, a simple property of the quantum mechanical system, it is possible to obtain the external potential and therefore the many-body wave-function. The wave-function, by its turn, determines every observable of the system. This implies that *every observable can be written as a functional of the density.*

Unfortunately, it is very hard to obtain the density of an interacting system. To circumvent this problem, Kohn and Sham introduced an auxiliary system of non-interacting particles[7]. The dynamics of these particles are governed by a potential chosen such that the density of the Kohn-Sham system equals the density of the interacting system. This potential is local (multiplicative) in real space, but it has a highly non-local functional dependence on the density. In non-mathematical terms this means that the potential at the point $\boldsymbol{r}$ can depend on the density of all other points (e.g. through gradients, or through integral operators like the Hartree potential). As we are now dealing with non-interacting particles, the Kohn-Sham equations are quite simple to solve numerically. However, the complexities of the many-body system are still present in the so-called exchange-correlation (xc) functional that needs to be approximated in any application of the theory.

2.2 The Runge-Gross theorem

In this section, we will present a detailed proof of the Runge-Gross theorem[5], the time-dependent extension of the ordinary Hohenberg-Kohn theorem[6]. There are several "technical" differences between a time-dependent and a static quantum-mechanical problem that one should keep in mind while trying to prove the Runge-Gross theorem. In static quantum mechanics, the ground-state of the system can be determined through the minimization of the total energy functional

$$E[\Phi] = \langle \Phi | \, \hat{H} \, | \Phi \rangle \ . \tag{7}$$

In time-dependent systems, there is no variational principle on the basis of the total energy for it is not a conserved quantity. There exists, however, a quantity analogous to the energy, the quantum mechanical action

$$\mathcal{A}[\Phi] = \int_{t_0}^{t_1} dt \ \langle \Phi(t) | \, i \frac{\partial}{\partial t} - \hat{H}(t) \, | \Phi(t) \rangle \ , \tag{8}$$

where $\Phi(t)$ is a N_{e}-body function defined in some convenient space. From expression (8) it is easy to obtain two important properties of the action: i) Equating the functional derivative of Eq. (8) in terms of $\Phi^*(t)$ to zero, we arrive at the time-dependent Schrödinger equation. We can therefore solve the time-dependent problem by calculating the stationary point of the functional $\mathcal{A}[\Phi]$. The function $\Psi(t)$ that makes the functional stationary will be the solution of the time-dependent many-body Schrödinger equation. Note that there is no "minimum principle", but only a "stationary principle". ii) The action is always zero at the solution point, i.e. $\mathcal{A}[\Psi] = 0$. These two properties make the quantum-mechanical action a much less useful quantity than its static counterpart, the total energy.

Another important point, often overlooked in the literature, is that a time-dependent problem in quantum mechanics is mathematically defined as an *initial value* problem. This stems from the fact that the time-dependent Schrödinger equation is a first-order differential equation in the time coordinate. The wave-function (or the density) thus depends on the initial state, which implies that the Runge-Gross theorem can only hold for a *fixed* initial state (and that the xc potential depends on that state). In contrast, the static Schrödinger equation is a second order differential equation in the space coordinates, and is the typical example of a *boundary value* problem.

From the above considerations the reader could conjecture that the proof of the Runge-Gross theorem is more involved than the proof of the ordinary Hohenberg-Kohn theorem. This is indeed the case. What we have to demonstrate is that if two potentials, $v(\boldsymbol{r}, t)$ and $v'(\boldsymbol{r}, t)$, differ by more than a purely time dependent function $c(t)$[2], they cannot produce the same time-dependent

[2] If the two potentials differ solely by a time-dependent function, they will produce wave-functions which are equal up to a purely time-dependent phase. This phase

density, $n(\boldsymbol{r},t)$, i.e.

$$v(\boldsymbol{r},t) \neq v'(\boldsymbol{r},t) + c(t) \Rightarrow \rho(\boldsymbol{r},t) \neq \rho'(\boldsymbol{r},t)\,. \tag{9}$$

This statement immediately implies the one-to-one correspondence between the potential and the density. In the following we will utilize primes to distinguish the quantities of the systems with external potentials v and v'. Due to technical reasons that will become evident during the course of the proof, we will have to restrict ourselves to external potentials that are Taylor expandable with respect to the time coordinate around the initial time t_0

$$v(\boldsymbol{r},t) = \sum_{k=0}^{\infty} c_k(\boldsymbol{r})(t-t_0)^k\,, \tag{10}$$

with the expansion coefficients

$$c_k(\boldsymbol{r}) = \left.\frac{1}{k!}\frac{d^k}{dt^k} v(\boldsymbol{r},t)\right|_{t=t_0}. \tag{11}$$

We furthermore define the function

$$u_k(\boldsymbol{r}) = \left.\frac{\partial^k}{\partial t^k}\left[v(\boldsymbol{r},t) - v'(\boldsymbol{r},t)\right]\right|_{t=t_0}. \tag{12}$$

Clearly, if the two potentials are different by more than a purely time-dependent function, at least one of the expansion coefficients in their Taylor expansion around t_0 will differ by more than a constant

$$\exists_{k\geq 0} : u_k(\boldsymbol{r}) \neq \text{const.} \tag{13}$$

In the first step of our proof we will demonstrate that if $v \neq v' + c(t)$ then the current densities, $\boldsymbol{j}$ and $\boldsymbol{j}'$, generated by v and v' are also different. The current density $\boldsymbol{j}$ can be written as the expectation value of the current density operator:

$$\boldsymbol{j}(\boldsymbol{r},t) = \langle\Psi(t)|\,\hat{\boldsymbol{j}}(\boldsymbol{r})\,|\Psi(t)\rangle\,, \tag{14}$$

where the operator $\hat{\boldsymbol{j}}$ is written

$$\hat{\boldsymbol{j}}(\boldsymbol{r}) = -\frac{1}{2\mathrm{i}}\left\{\left[\nabla\hat{\psi}^\dagger(\boldsymbol{r})\right]\hat{\psi}(\boldsymbol{r}) - \hat{\psi}^\dagger(\boldsymbol{r})\left[\nabla\hat{\psi}(\boldsymbol{r})\right]\right\}. \tag{15}$$

We now use the quantum-mechanical equation of motion, which is valid for any operator, $\hat{O}(t)$,

$$\mathrm{i}\frac{d}{dt}\langle\Psi(t)|\,\hat{O}(t)\,|\Psi(t)\rangle = \langle\Psi(t)|\,\mathrm{i}\frac{\partial}{\partial t}\hat{O}(t) + \left[\hat{O}(t),\hat{H}(t)\right]|\Psi(t)\rangle\,, \tag{16}$$

will, of course, cancel while calculating the density (or any other observable, in fact).

to write the equation of motion for the current density in the primed and unprimed systems

$$\mathrm{i}\frac{d}{dt}\boldsymbol{j}(\boldsymbol{r},t) = \langle\Psi(t)|\left[\hat{\boldsymbol{j}}(\boldsymbol{r}),\hat{H}(t)\right]|\Psi(t)\rangle \tag{17}$$

$$\mathrm{i}\frac{d}{dt}\boldsymbol{j}'(\boldsymbol{r},t) = \langle\Psi'(t)|\left[\hat{\boldsymbol{j}}(\boldsymbol{r}),\hat{H}'(t)\right]|\Psi'(t)\rangle\ . \tag{18}$$

As we start from a fixed initial many-body state, at t_0 the wave-functions, the densities, and the current densities have to be equal in the primed and unprimed systems

$$|\Psi(t_0)\rangle = |\Psi'(t_0)\rangle \equiv |\Psi_0\rangle \tag{19}$$

$$n(\boldsymbol{r},t_0) = n'(\boldsymbol{r},t_0) \equiv n_0(\boldsymbol{r}) \tag{20}$$

$$\boldsymbol{j}(\boldsymbol{r},t_0) = \boldsymbol{j}'(\boldsymbol{r},t_0) \equiv \boldsymbol{j}_0(\boldsymbol{r})\,. \tag{21}$$

If we now take the difference between the equations of motion (17) and (18) we obtain, when $t = t_0$,

$$\begin{aligned}\mathrm{i}\frac{d}{dt}\left[\boldsymbol{j}(\boldsymbol{r},t)-\boldsymbol{j}'(\boldsymbol{r},t)\right]_{t=t_0} &= \langle\Psi_0|\left[\hat{\boldsymbol{j}}(\boldsymbol{r}),\hat{H}(t_0)-\hat{H}'(t_0)\right]|\Psi_0\rangle \\ &= \langle\Psi_0|\left[\hat{\boldsymbol{j}}(\boldsymbol{r}),v(\boldsymbol{r},t_0)-v'(\boldsymbol{r},t_0)\right]|\Psi_0\rangle \\ &= \mathrm{i}n_0(\boldsymbol{r})\nabla\left[v(\boldsymbol{r},t_0)-v'(\boldsymbol{r},t_0)\right]\ .\end{aligned} \tag{22}$$

Let us assume that Eq. (13) is fulfilled already for $k = 0$, i.e. that the two potentials, v and v', differ at t_0. This immediately implies that the derivative on the left-hand side of Eq. (22) differs from zero. The two current densities $\boldsymbol{j}$ and $\boldsymbol{j}'$ will consequently deviate for $t > t_0$. If k is greater than zero the equation of motion is applied $k+1$ times to yield

$$\frac{d^{k+1}}{dt^{k+1}}\left[\boldsymbol{j}(\boldsymbol{r},t)-\boldsymbol{j}'(\boldsymbol{r},t)\right]_{t=t_0} = n_0(\boldsymbol{r})\nabla u_k(\boldsymbol{r})\,. \tag{23}$$

The right-hand side of Eq. (23) differs from zero, which again implies that $\boldsymbol{j}(\boldsymbol{r},t) \neq \boldsymbol{j}'(\boldsymbol{r},t)$ for $t > t_0$.

In a second step we prove that $\boldsymbol{j} \neq \boldsymbol{j}'$ implies $n \neq n'$. To achieve that purpose we will make use of the continuity equation

$$\frac{\partial}{\partial t}n(\boldsymbol{r},t) = -\nabla\cdot\boldsymbol{j}(\boldsymbol{r},t)\,. \tag{24}$$

If we write Eq. (24) for the primed and unprimed system and take the difference, we arrive at

$$\frac{\partial}{\partial t}\left[n(\boldsymbol{r},t)-n'(\boldsymbol{r},t)\right] = -\nabla\cdot\left[\boldsymbol{j}(\boldsymbol{r},t)-\boldsymbol{j}'(\boldsymbol{r},t)\right]\ . \tag{25}$$

As before, we would like an expression involving the kth time derivative of the external potential. We therefore take the $(k+1)$st time-derivative of the previous equation to obtain (at $t = t_0$)

$$\frac{\partial^{k+2}}{\partial t^{k+2}} \left[n(\boldsymbol{r},t) - n'(\boldsymbol{r},t)\right]_{t=t_0} = -\nabla \cdot \frac{\partial^{k+1}}{\partial t^{k+1}} \left[\boldsymbol{j}(\boldsymbol{r},t) - \boldsymbol{j}'(\boldsymbol{r},t)\right]_{t=t_0} = -\nabla \cdot \left[n_0(\boldsymbol{r}) \nabla u_k(\boldsymbol{r})\right] . \tag{26}$$

In the last step we made use of Eq. (23). By the hypothesis (13) we have $u_k(\boldsymbol{r}) \neq$ const. hence it is clear that if

$$\nabla \cdot \left[n_0(\boldsymbol{r}) \nabla u_k(\boldsymbol{r})\right] \neq 0 \,, \tag{27}$$

then $n \neq n'$, from which follows the Runge-Gross theorem. To show that Eq. (27) is indeed fulfilled, we will use the versatile technique of demonstration by *reductio ad absurdum*. Let us assume that $\nabla \cdot [n_0(\boldsymbol{r}) \nabla u_k(\boldsymbol{r})] = 0$ with $u_k(\boldsymbol{r}) \neq$ const., and look at the integral

$$\int d^3r \, n_0(\boldsymbol{r}) \left[\nabla u_k(\boldsymbol{r})\right]^2 = -\int d^3r \, u_k(\boldsymbol{r}) \nabla \cdot \left[n_0(\boldsymbol{r}) \nabla u_k(\boldsymbol{r})\right] + \int_{\mathrm{S}} n_0(\boldsymbol{r}) u_k(\boldsymbol{r}) \nabla u_k(\boldsymbol{r}) \cdot d\boldsymbol{S} \,. \tag{28}$$

This equality was obtained with the help of Green's theorem. The first term on the right-hand side is zero by assumption, while the second term vanishes if the density and the function $u_k(\boldsymbol{r})$ decay in a "reasonable" manner when $r \to \infty$. This situation is always true for finite systems. We further notice that the integrand $n_0(\boldsymbol{r}) \left[\nabla u_k(\boldsymbol{r})\right]^2$ is always positive. These diverse conditions can only be satisfied if either the density n_0 or $\nabla u_k(\boldsymbol{r})$ vanish identically. The first possibility is obviously ruled out, while the second contradicts our initial assumption that $u_k(\boldsymbol{r})$ is not a constant. This concludes the proof of the Runge-Gross theorem.

2.3 Time-dependent Kohn-Sham equations

As mentioned in section 2.1, the Runge-Gross theorem asserts that all observables can be calculated with the knowledge of the one-body density. Nothing is however stated on how to calculate that valuable quantity. To circumvent the cumbersome task of solving the interacting Schrödinger equation, Kohn and Sham had the idea of utilizing an auxiliary system of non-interacting (Kohn-Sham) electrons, subject to an external local potential, v_{KS}[7]. This potential is unique, by virtue of the Runge-Gross theorem applied to the non-interacting system, and is chosen such that the density of the Kohn-Sham electrons is the same as the density of the original interacting system. In the time-dependent case, these Kohn-Sham electrons obey the time-dependent

Schrödinger equation

$$\mathrm{i}\frac{\partial}{\partial t}\varphi_i(\boldsymbol{r},t) = \left[-\frac{\nabla^2}{2} + v_{\mathrm{KS}}(\boldsymbol{r},t)\right]\varphi_i(\boldsymbol{r},t)\,. \tag{29}$$

The density of the interacting system can be obtained from the time-dependent Kohn-Sham orbitals

$$n(\boldsymbol{r},t) = \sum_i^{\mathrm{occ}} |\varphi_i(\boldsymbol{r},t)|^2\,. \tag{30}$$

Eq. (29), having the form of a one-particle equation, is fairly easy to solve numerically. We stress, however, that the Kohn-Sham equation *is not* a mean-field approximation: If we knew the exact Kohn-Sham potential, v_{KS}, we would obtain from Eq. (29) the exact Kohn-Sham orbitals, and from these the correct density of the system.

The Kohn-Sham potential is conventionally separated in the following way

$$v_{\mathrm{KS}}(\boldsymbol{r},t) = v_{\mathrm{ext}}(\boldsymbol{r},t) + v_{\mathrm{Hartree}}(\boldsymbol{r},t) + v_{\mathrm{xc}}(\boldsymbol{r},t)\,. \tag{31}$$

The first term is again the external potential. The Hartree potential accounts for the classical electrostatic interaction between the electrons

$$v_{\mathrm{Hartree}}(\boldsymbol{r},t) = \int d^3r'\,\frac{n(\boldsymbol{r},t)}{|\boldsymbol{r}-\boldsymbol{r}'|}\,. \tag{32}$$

The last term, the xc potential, comprises all the non-trivial many-body effects. In ordinary DFT, v_{xc} is normally written as a functional derivative of the xc energy. This follows from a variational derivation of the Kohn-Sham equations starting from the total energy. It is not straightforward to extend this formulation to the time-dependent case due to a problem related to causality[11,2]. The problem was solved by van Leeuwen in 1998, by using the Keldish formalism to defined a new action functional[12], $\tilde{\mathcal{A}}$. The time-dependent xc potential can then be written as the functional derivative of the xc part of $\tilde{\mathcal{A}}$,

$$v_{\mathrm{xc}}(\boldsymbol{r},t) = \left.\frac{\delta\tilde{\mathcal{A}}_{\mathrm{xc}}}{\delta n(\boldsymbol{r},\tau)}\right|_{n(\boldsymbol{r},t)}\,, \tag{33}$$

where τ stands for the Keldish pseudo-time.

Inevitably, the exact expression of v_{xc} as a functional of the density is unknown. At this point we are obliged to perform an approximation. It is important to stress that this is the *only* fundamental approximation in TDDFT. In contrast to stationary-state DFT, where very good xc functionals exist, approximations to $v_{\mathrm{xc}}(\boldsymbol{r},t)$ are still in their infancy. The first and simplest of these is the adiabatic local density approximation (ALDA), reminiscent of the ubiquitous LDA. More recently, several other functionals were proposed, from which we mention the time-dependent exact-exchange (EXX) functional[13], and the attempt by Dobson, Bünner, and Gross[14] to construct an xc functional with memory. In the following section we will introduce the above mentioned functionals.

2.4 xc functionals

Adiabatic approximations There is a very simple procedure that allows the use of the plethora of existing xc functionals for ground-state DFT in the time-dependent theory. Let us assume that $\tilde{v}_{\rm xc}[n]$ is an approximation to the ground-state xc density functional. We can write an adiabatic time-dependent xc potential as

$$v_{\rm xc}^{\rm adiabatic}(\boldsymbol{r},t) = \tilde{v}_{\rm xc}[n](\boldsymbol{r})|_{n=n(t)} \; . \tag{34}$$

I.e. we employ the same functional form but evaluated at each time with the density $n(\boldsymbol{r},t)$. The functional thus constructed is obviously local in time. This is, of course, a quite dramatic approximation. The functional $\tilde{v}_{\rm xc}[n]$ is a ground-state property, so we expect the adiabatic approximation to work only in cases where the temporal dependence is small, i.e., when our time-dependent system is locally close to equilibrium. Certainly this is not the case if we are studying the interaction of strong laser pulses with matter.

By inserting the LDA functional in Eq. (34) we obtain the so-called adiabatic local density approximation (ALDA)

$$v_{\rm xc}^{\rm ALDA}(\boldsymbol{r},t) = v_{\rm xc}^{\rm HEG}(n)\big|_{n=n(\boldsymbol{r},t)} \; . \tag{35}$$

The ALDA assumes that the xc potential at the point $\boldsymbol{r}$, and time t is equal to the xc potential of a (static) homogeneous-electron gas (HEG) of density $n(\boldsymbol{r},t)$. Naturally, the ALDA retains all problems already present in the LDA. Of these, we would like to emphasize the erroneous asymptotic behavior of the LDA xc potential: For neutral finite systems, the exact xc potential decays as $-1/r$, whereas the LDA xc potential falls off exponentially. Note that most of the generalized-gradient approximations (GGAs), or even the newest meta-GGAs have asymptotic behaviors similar to the LDA. This problem gains particular relevance when calculating ionization yields (the ionization potential calculated with the ALDA is always too small), or in situations where the electrons are pushed to regions far away from the nuclei (e.g., by a strong laser) and feel the incorrect tail of the potential.

Despite this problem, the ALDA yields remarkably good excitation energies (see sections 4.2 and 4.3) and is probably the most used xc functional in TDDFT.

Time-dependent optimized effective potential Unfortunately, when one is trying to write $v_{\rm xc}$ as explicit functionals of the density, one encounters some difficulties. As an alternative, the so-called orbital-dependent xc functionals were introduced several years ago. These functionals are written explicitly in terms of the Kohn-Sham orbitals, albeit remaining *implicit* density functionals by virtue of the Runge-Gross theorem. A typical member of this family is the exact-exchange (EXX) functional. The EXX action is obtained by expanding $\mathcal{A}_{\rm xc}$ in powers of e^2 (where e is the electronic charge),

and retaining the lowest order term, the exchange term. It is given by the Fock integral

$$\mathcal{A}_{\mathrm{x}}^{\mathrm{EXX}} = -\frac{1}{2}\sum_{j,k}^{\mathrm{occ}}\int_{t_0}^{t_1} dt \int d^3r \int d^3r' \, \frac{\varphi_j^*(\boldsymbol{r}',t)\varphi_k(\boldsymbol{r}',t)\varphi_j(\boldsymbol{r},t)\varphi_k^*(\boldsymbol{r},t)}{|\boldsymbol{r}-\boldsymbol{r}'|} \,. \quad (36)$$

From such an action functional, one seeks to determine the local Kohn-Sham potential through a series of chain rules for functional derivatives. The procedure is called the optimized effective potential (OEP) or the optimized potential method (OPM) for historical reasons[15,16]. The derivation of the time-dependent version of the OEP equations is very similar to the ground-state case. Due to space limitations we will not present the derivation in this article. The interested reader is advised to consult the original paper[13], one of the more recent publications[17,18], or the chapter by E. Engel contained in this volume. The final form of the OEP equation that determines the EXX potential is

$$\begin{aligned} 0 = \sum_{j}^{\mathrm{occ}} \int_{-\infty}^{t_1} dt' \int d^3r' \quad & [v_{\mathrm{x}}(\boldsymbol{r}',t') - u_{\mathrm{x}\,j}(\boldsymbol{r}',t')] \\ & \times\varphi_j(\boldsymbol{r},t)\varphi_j^*(\boldsymbol{r}',t')G_{\mathrm{R}}(\boldsymbol{r}t,\boldsymbol{r}'t') + \mathrm{c.c.} \end{aligned} \quad (37)$$

The kernel, G_{R}, is defined by

$$\mathrm{i}G_{\mathrm{R}}(\boldsymbol{r}t,\boldsymbol{r}'t') = \sum_{k=1}^{\infty}\varphi_k^*(\boldsymbol{r},t)\varphi_k(\boldsymbol{r}',t')\theta(t-t') \,, \quad (38)$$

and can be identified with the retarded Green's function of the system. Moreover, the expression for u_{x} is essentially the functional derivative of the xc action in relation to the Kohn-Sham wave-functions

$$u_{\mathrm{x}\,j}(\boldsymbol{r},t) = \frac{1}{\varphi_j^*(\boldsymbol{r},t)}\frac{\delta\mathcal{A}_{\mathrm{xc}}[\varphi_j]}{\delta\varphi_j(\boldsymbol{r},t)} \,. \quad (39)$$

Note that the xc potential is still a local potential, albeit being obtained through the solution of an extremely non-local and non-linear integral equation. In reality, the solution of Eq. (37) poses a very difficult numerical problem. Fortunately, by performing an approximation first proposed by Krieger, Li, and Iafrate (KLI) it is possible to simplify the whole procedure, and obtain an semi-analytic solution of Eq. (37)[19]. The KLI approximation turns out to be a very good approximation to the EXX potential. Note that both the EXX and the KLI potential have the correct $-1/r$ asymptotic behavior for neutral finite systems.

A functional with memory There is a very common procedure for the construction of approximate xc functionals in ordinary DFT. It starts with

the derivation of *exact* properties of $v_{\rm xc}$, deemed important by physical arguments. Then an analytical expression for the functional is proposed, such that it satisfies those rigorous constraints. We will use this recipe to generate a time-dependent xc potential which is non-local in time, i.e. that includes the "memory" from previous times[14].

A very important condition comes from Galilean invariance. Let us look at a system from the point of view of a moving reference frame whose origin is given by $\boldsymbol{x}(t)$. The density seen from this moving frame is simply the density of the reference frame, but shifted by $\boldsymbol{x}(t)$

$$n'(\boldsymbol{r},t) = n(\boldsymbol{r}-\boldsymbol{x}(t),t)\,. \tag{40}$$

Galilean invariance then implies[20]

$$v_{\rm xc}[n'](\boldsymbol{r},t) = v_{\rm xc}[n](\boldsymbol{r}-\boldsymbol{x}(t),t)\,. \tag{41}$$

It is obvious that potentials that are both local in space and in time, like the ALDA, trivially fulfill this requirement. However, when one tries to deduce an xc potential which is non-local in time, one finds condition (41) quite difficult to satisfy.

Another rigorous constraint follows from Ehrenfest's theorem which relates the acceleration to the gradient of the external potential

$$\frac{d^2}{dt^2}\langle \boldsymbol{r}\rangle = -\langle \nabla v_{\rm ext}(\boldsymbol{r})\rangle\ . \tag{42}$$

For an interacting system, Ehrenfest's theorem states

$$\frac{d^2}{dt^2}\int d^3r\,\boldsymbol{r}\ n(\boldsymbol{r},t) = -\int d^3r\, n(\boldsymbol{r},t)\nabla v_{\rm ext}(\boldsymbol{r})\,. \tag{43}$$

In the same way we can write Ehrenfest's theorem for the Kohn-Sham system

$$\frac{d^2}{dt^2}\int d^3r\,\boldsymbol{r}\ n(\boldsymbol{r},t) = -\int d^3r\, n(\boldsymbol{r},t)\nabla v_{\rm KS}(\boldsymbol{r})\,. \tag{44}$$

By the construction of the Kohn-Sham system, the interacting density is equal to the Kohn-Sham density. We can therefore equate the right-hand sides of Eq. (43) and (44), and arrive at

$$\int d^3r\, n(\boldsymbol{r},t)\nabla v_{\rm ext}(\boldsymbol{r}) = \int d^3r\, n(\boldsymbol{r},t)\nabla v_{\rm KS}(\boldsymbol{r},t)\,. \tag{45}$$

If we now insert the definition of the Kohn-Sham potential, Eq. 31, and note that $\int d^3r\, n(\boldsymbol{r},t)\nabla v_{\rm Hartree}(\boldsymbol{r}) = 0$, we obtain the condition

$$\int d^3r\, n(\boldsymbol{r},t)\nabla v_{\rm xc}(\boldsymbol{r},t) = \int d^3r\, n(\boldsymbol{r},t)\boldsymbol{F}_{\rm xc}(\boldsymbol{r},t) = 0\,, \tag{46}$$

i.e. the total xc force of the system is zero. This condition reflects Newton's third law: The xc effects are only due to internal forces, the Coulomb interaction among the electrons, and should not give rise to any net force on the system.

A functional that takes into account these exact constraints can be constructed[14]. The condition (46) is simply ensured by the expression

$$\boldsymbol{F}_{\rm xc}(\boldsymbol{r},t) = \frac{1}{n(\boldsymbol{r},t)}\nabla \int dt' \Pi_{\rm xc}(n(\boldsymbol{r},t'),t-t')\,. \tag{47}$$

The function $\Pi_{\rm xc}$ is a pressure-like scalar memory function of two variables. In practice, $\Pi_{\rm xc}$ is fully determined by requiring it to reproduce the scalar linear response of the homogeneous electron gas. Expression (47) is clearly non-local in the time-domain but still local in the spatial coordinates. From the previous considerations it is clear that it must violate Galilean invariance. To correct this problem we use a concept borrowed from hydrodynamics. It is assumed that, in the electron liquid, memory resides not with each fixed point $\boldsymbol{r}$, but rather within each separate "fluid element". Thus the element which arrives at location $\boldsymbol{r}$ at time t "remembers" what happened to it at earlier times t' when it was at locations $\boldsymbol{R}(t'|\boldsymbol{r},t)$, different from its present location $\boldsymbol{r}$. The trajectory, $\boldsymbol{R}$, can be determined by demanding that its time derivative equals the fluid velocity

$$\frac{\partial}{\partial t'}\boldsymbol{R}(t'|\boldsymbol{r},t) = \frac{\boldsymbol{j}(\boldsymbol{R},t')}{n(\boldsymbol{R},t')}\,, \tag{48}$$

with the boundary condition

$$\boldsymbol{R}(t|\boldsymbol{r},t) = \boldsymbol{r}\,. \tag{49}$$

We then correct the Eq. (47) by evaluating n at point $\boldsymbol{R}$

$$\boldsymbol{F}_{\rm xc}(\boldsymbol{r},t) = \frac{1}{n(\boldsymbol{r},t)}\nabla \int dt' \Pi_{\rm xc}(n(\boldsymbol{R},t'),t-t')\,. \tag{50}$$

Finally, an expression for $v_{\rm xc}$ can be obtained by direct integration of $\boldsymbol{F}_{\rm xc}$ (see [14] for details).

2.5 Numerical considerations

As mentioned before, the solution of the time-dependent Kohn-Sham equations is an initial value problem. At $t = t_0$ the system is in some initial state described by the Kohn-Sham orbitals $\varphi_i(\boldsymbol{r},t_0)$. In most cases the initial state will be the ground state of the system (i.e., $\varphi_i(\boldsymbol{r},t_0)$ will be the solution of the ground-state Kohn-Sham equations). The main task of the computational physicist is then to propagate this initial state until some final time, t_f.

The time-dependent Kohn-Sham equations can be rewritten in the integral form

$$\varphi_i(\boldsymbol{r}, t_f) = \hat{U}(t_f, t_0)\varphi_i(\boldsymbol{r}, t_0)\,, \tag{51}$$

where the time-evolution operator, $\hat{U}$, is defined by

$$\hat{U}(t', t) = \hat{T} \exp\left[-\mathrm{i}\int_t^{t'} d\tau\ \hat{H}_{\mathrm{KS}}(\tau)\right]\,. \tag{52}$$

Note that $\hat{H}_{\mathrm{KS}}$ is explicitly time-dependent due to the Hartree and xc potentials. It is therefore important to retain the time-ordering propagator, $\hat{T}$, in the definition of the operator $\hat{U}$. The exponential in expression (52) is clearly too complex to be applied directly, and needs to be approximated in some suitable manner. To reduce the error in the propagation from t_0 to t_f, this large interval is usually split into smaller sub-intervals of length $\Delta\, t$. The wave-functions are then propagated from $t_0 \rightarrow t_0 + \Delta\, t$, then from $t_0 + \Delta\, t \rightarrow t_0 + 2\Delta\, t$ and so on.

The simplest approximation to (56) is a direct expansion of the exponential in a power series of $\Delta\, t$

$$\hat{U}(t + \Delta\, t, t) \approx \sum_{l=0}^{k} \frac{\left[-\mathrm{i}\hat{H}(t + \Delta\, t/2)\Delta\, t\right]^l}{l!} + \mathcal{O}(\Delta\, t^{k+1})\,. \tag{53}$$

Unfortunately, the expression (53) does not retain one of the most important properties of the Kohn-Sham time-evolution operator: unitarity. In other words, if we apply Eq. (53) to a normalized wave-function the result will no longer be normalized. This leads to an inherently unstable propagation. Several propagation methods that fulfill the condition of unitarity exist in the market. We will briefly mention two of these: a modified Krank-Nicholson scheme, and the split-operator method.

A modified Krank-Nicholson scheme This method is derived by imposing time-reversal symmetry to an approximate time-evolution operator. It is clear that we can obtain the state at time $t + \Delta\, t/2$ either by forward propagating the state at t by $\Delta\, t/2$, or by backward propagating the state at $t + \Delta\, t$

$$\begin{aligned}\varphi(t + \Delta\, t/2) &= \hat{U}(t + \Delta\, t/2, t)\varphi(t) \\ &= \hat{U}(t - \Delta\, t/2, t + \Delta\, t)\varphi(t + \Delta\, t)\,.\end{aligned} \tag{54}$$

This equality leads to

$$\varphi(t + \Delta\, t) = \hat{U}(t + \Delta\, t/2, t + \Delta\, t)\hat{U}(t + \Delta\, t/2, t)\varphi(t)\,, \tag{55}$$

where we used the fact that the inverse of the time-evolution operator $\hat{U}^{-1}(t+\Delta t, t) = \hat{U}(t-\Delta t, t)$. To propagate a state from t to $t+\Delta t$ we follow the steps:

i) Obtain an estimate of the Kohn-Sham wave-functions at time $t + \Delta t$ by propagating from time t using a "low quality" formula for $\hat{U}(t + \Delta t, t)$. The expression (53) expanded to third or forth order is well suited for this purpose. ii) With these wave-functions construct an approximation to $\hat{H}(t + \Delta t)$ and to $\hat{U}(t + \Delta t/2, t + \Delta t)$. iii) Apply Eq. (55). This procedure leads to a very stable propagation.

The split-operator method In a first step we neglect the time-ordering in Eq. (52), and approximate the integral in the exponent by a trapezoidal rule

$$\hat{U}(t + \Delta t, t) \approx \exp\left[-\mathrm{i}\hat{H}_{\mathrm{KS}}(t)\Delta t\right] = \exp\left[-\mathrm{i}(\hat{T} + \hat{V}_{\mathrm{KS}})\Delta t\right] . \tag{56}$$

We note that the operators $\exp\left(-\mathrm{i}\hat{V}_{\mathrm{KS}}\Delta t\right)$ and $\exp\left(-\mathrm{i}\hat{T}\Delta t\right)$ are diagonal respectively in real and Fourier spaces, and therefore trivial to apply in those spaces. It is possible to decompose the exponential (56) into a form involving only these two operators. The two lowest order decompositions are

$$\exp\left[-\mathrm{i}(\hat{T} + \hat{V}_{\mathrm{KS}})\Delta t\right] = \exp\left(-\mathrm{i}\hat{T}\Delta t\right)\exp\left(-\mathrm{i}\hat{V}_{\mathrm{KS}}\Delta t\right) + \mathcal{O}(\Delta t^2) \tag{57}$$

and

$$\exp\left[-\mathrm{i}(\hat{T} + \hat{V}_{\mathrm{KS}})\Delta t\right] = \exp\left(-\mathrm{i}\hat{T}\frac{\Delta t}{2}\right)\exp\left(-\mathrm{i}\hat{V}_{\mathrm{KS}}\Delta t\right)\exp\left(-\mathrm{i}\hat{T}\frac{\Delta t}{2}\right) + \mathcal{O}(\Delta t^3) . \tag{58}$$

For example, to apply the splitting (58) to $\varphi(\boldsymbol{r}, t)$ we start by Fourier transforming the wave-function to Fourier space. We then apply $\exp\left(-\mathrm{i}\hat{T}\frac{\Delta t}{2}\right)$ to $\varphi(\boldsymbol{k}, t)$ and Fourier transform back the result to real space. We proceed by applying $\exp\left(-\mathrm{i}\hat{V}\Delta t\right)$, Fourier transforming, etc. This method can be made very efficient by the use of fast-Fourier transforms.

As a better approximation to the propagator (52) we can use a mid-point rule to estimate the integral in the exponential

$$\hat{U}(t + \Delta t, t) \approx \exp\left[-\mathrm{i}\hat{H}_{\mathrm{KS}}(t + \Delta t/2)\Delta t\right] . \tag{59}$$

It can be shown that the same procedure described above can be applied with only a slight modification: The Kohn-Sham potential has to be updated after applying the first kinetic operator [21].

3 Linear response theory

3.1 Basic theory

In circumstances where the external time-dependent potential is small, it may not be necessary to solve the full time-dependent Kohn-Sham equations.

Instead perturbation theory may prove sufficient to determine the behavior of the system. We will focus on the linear change of the density, that allows us to calculate, e.g., the optical absorption spectrum.

Let us assume that for $t < t_0$ the time-dependent potential $v_{\rm TD}$ is zero – i.e. the system is subject only to the nuclear potential, $v^{(0)}$ – and furthermore that the system is in its ground-state with ground-state density $n^{(0)}$. At t_0 we turn on the perturbation, $v^{(1)}$, so that the total external potential now consists of $v_{\rm ext} = v^{(0)} + v^{(1)}$. Clearly $v^{(1)}$ will induce a change in the density. If the perturbing potential is sufficiently well-behaved (like almost always in physics), we can expand the density in a perturbative series

$$n(\boldsymbol{r},t) = n^{(0)}(\boldsymbol{r}) + n^{(1)}(\boldsymbol{r},t) + n^{(2)}(\boldsymbol{r},t) + \cdots \tag{60}$$

where $n^{(1)}$ is the component of $n(\boldsymbol{r},t)$ that depends linearly on $v^{(1)}$, $n^{(2)}$ depends quadratically, etc. As the perturbation is weak, we will only be concerned with the linear term, $n^{(1)}$. In frequency space it reads

$$n^{(1)}(\boldsymbol{r},\omega) = \int d^3\boldsymbol{r}'\, \chi(\boldsymbol{r},\boldsymbol{r}',\omega) v^{(1)}(\boldsymbol{r}',\omega)\,. \tag{61}$$

The quantity χ is the linear density-density response function of the system. In other branches of physics it has other names, e.g., in the context of many-body perturbation theory it is called the reducible polarization function. Unfortunately, the evaluation of χ through perturbation theory is a very demanding task. We can, however, make use of TDDFT to simplify this process.

We recall that in the time-dependent Kohn-Sham framework, the density of the *interacting* system of electrons is obtained from a fictitious system of *non-interacting* electrons. Clearly, we can also calculate the linear change of density using the Kohn-Sham system

$$n^{(1)}(\boldsymbol{r},\omega) = \int d^3\boldsymbol{r}'\, \chi_{\rm KS}(\boldsymbol{r},\boldsymbol{r}',\omega) v^{(1)}_{\rm KS}(\boldsymbol{r}',\omega)\,. \tag{62}$$

Note that the response function that enters Eq. (62), $\chi_{\rm KS}$, is the density response function of a system of *non-interacting* electrons and is, consequently, much easier to calculate than the full interacting χ. In terms of the unperturbed stationary Kohn-Sham orbitals it reads

$$\chi_{\rm KS}(\boldsymbol{r},\boldsymbol{r}',\omega) = \lim_{\eta\to 0^+} \sum_{jk}^{\infty} (f_k - f_j)\, \frac{\varphi_j(\boldsymbol{r})\varphi_j^*(\boldsymbol{r}')\varphi_k(\boldsymbol{r}')\varphi_k^*(\boldsymbol{r})}{\omega - (\epsilon_j - \epsilon_k) + i\eta}\,, \tag{63}$$

where f_m is the occupation number of the m orbital in the Kohn-Sham ground-state. Note that the Kohn-Sham potential, $v_{\rm KS}$, includes all powers of the external perturbation due to its non-linear dependence on the density. The potential that enters Eq. (62) is however just the *linear* change of $v_{\rm KS}$,

$v^{(1)}_{\rm KS}$. This latter quantity can be calculated explicitly from the definition of the Kohn-Sham potential

$$v^{(1)}_{\rm KS}(\boldsymbol{r},t) = v^{(1)}(\boldsymbol{r},t) + v^{(1)}_{\rm Hartree}(\boldsymbol{r},t) + v^{(1)}_{\rm xc}(\boldsymbol{r},t)\,. \tag{64}$$

The variation of the external potential is simply $v^{(1)}$, while the change in the Hartree potential is

$$v^{(1)}_{\rm Hartree}(\boldsymbol{r},t) = \int d^3r'\,\frac{n^{(1)}(\boldsymbol{r}',t)}{|\boldsymbol{r}-\boldsymbol{r}'|}\,. \tag{65}$$

Finally $v^{(1)}_{\rm xc}(\boldsymbol{r},t)$ is the linear part in $n^{(1)}$ of the functional $v_{\rm xc}[n]$,

$$v^{(1)}_{\rm xc}(\boldsymbol{r},t) = \int dt' \int d^3r'\,\frac{\delta v_{\rm xc}(\boldsymbol{r},t)}{\delta n(\boldsymbol{r}',t')} n^{(1)}(\boldsymbol{r}',t')\,. \tag{66}$$

It is useful to introduce the exchange-correlation kernel, $f_{\rm xc}$, defined by

$$f_{\rm xc}(\boldsymbol{r}t,\boldsymbol{r}'t') = \frac{\delta v_{\rm xc}(\boldsymbol{r},t)}{\delta n(\boldsymbol{r}',t')}\,. \tag{67}$$

The kernel is a well know quantity that appears in several branches of theoretical physics. E.g., evaluated for the electron gas, $f_{\rm xc}$ is, up to a factor, the "local-field correction"; To emphasize the correspondence to the effective interaction of Landau's Fermi-liquid theory, $f_{\rm xc}$ plus the bare Coulomb interaction is sometimes called the "effective interaction", while in the theory of classical liquids the same quantity is referred to as the Ornstein-Zernicke function.

Combining the previous results, and transforming to frequency space we arrive at:

$$\begin{aligned} n^{(1)}(\boldsymbol{r},\omega) = &\int d^3r'\,\chi_{\rm KS}(\boldsymbol{r},\boldsymbol{r}',\omega) v^{(1)}(\boldsymbol{r}',\omega) \\ &+ \int d^3x \int d^3r'\,\chi_{\rm KS}(\boldsymbol{r},\boldsymbol{x},\omega)\left[\frac{1}{|\boldsymbol{x}-\boldsymbol{r}'|} + f_{\rm xc}(\boldsymbol{x},\boldsymbol{r}',\omega)\right] n^{(1)}(\boldsymbol{r}',\omega)\,. \end{aligned} \tag{68}$$

From Eq. (61) and Eq. (68) trivially follows the relation

$$\begin{aligned} \chi(\boldsymbol{r},\boldsymbol{r}',\omega) = &\chi_{\rm KS}(\boldsymbol{r},\boldsymbol{r}',\omega) + \\ &\int d^3x \int d^3x'\,\chi(\boldsymbol{r},\boldsymbol{x},\omega)\left[\frac{1}{|\boldsymbol{x}-\boldsymbol{x}'|} + f_{\rm xc}(\boldsymbol{x},\boldsymbol{x}',\omega)\right]\chi_{\rm KS}(\boldsymbol{x}',\boldsymbol{r}',\omega)\,. \end{aligned} \tag{69}$$

This equation is a formally exact representation of the linear density response in the sense that, if we possessed the exact Kohn-Sham potential (so that we could extract $f_{\rm xc}$), a self-consistent solution of (69) would yield the response function, χ, of the interacting system.

3.2 The xc kernel

As we have seen in the previous section, the main ingredient in linear response theory is the xc kernel. $f_{\rm xc}$, as expected, is a very complex quantity that includes – or, in other words, hides – all non-trivial many-body effects. Many approximate xc kernels have been proposed in the literature over the past years. The most ancient, and certainly the simplest is the ALDA kernel

$$f_{\rm xc}^{\rm ALDA}(\boldsymbol{r}t,\boldsymbol{r}'t') = \delta(\boldsymbol{r}-\boldsymbol{r}')\delta(t-t')\left.f_{\rm xc}^{\rm HEG}(n)\right|_{n=n(\boldsymbol{r},t)}\,, \tag{70}$$

where

$$f_{\rm xc}^{\rm HEG}(n) = \frac{d}{dn}v_{\rm xc}^{\rm HEG}(n) \tag{71}$$

is just the derivative of the xc potential of the homogeneous electron gas. The ALDA kernel is local both in the space and time coordinates.

Another commonly used xc kernel was derived by Petersilka *et al.* in 1996, and is nowadays referred to as the PGG kernel[22]. Its derivation starts from a simple analytic approximation to the EXX potential. This approximation, that is called the Slater approximation in the context of Hartree-Fock theory, only retains the leading term in the expression for EXX, which reads

$$v_{\rm x}^{\rm PGG}(\boldsymbol{r},t) = \sum_k^{\rm occ}\frac{|\varphi_k(\boldsymbol{r},t)|^2}{n(\boldsymbol{r},t)}\left[u_{{\rm x}\,k}(\boldsymbol{r},t) + {\rm c.c}\right]\,. \tag{72}$$

Using the definition (67) and after some algebra we arrive at the final form of the PGG kernel

$$f_{\rm x}^{\rm PGG}(\boldsymbol{r}t,\boldsymbol{r}'t') = -\delta(t-t')\frac{1}{2}\frac{1}{|\boldsymbol{r}-\boldsymbol{r}'|}\frac{\left|\sum_k^{\rm occ}\varphi_k(\boldsymbol{r})\varphi_k^*(\boldsymbol{r}')\right|^2}{n(\boldsymbol{r})n(\boldsymbol{r}')}\,. \tag{73}$$

As in the case of the ALDA, the PGG kernel is local in time .

Noticing the crudeness of the ALDA, especially the complete neglect of any frequency dependence, one could expect it to yield very inaccurate results in most situations. Surprisingly, this is not the case as we will show in section 4. To understand this numerical evidence, we have to take a step back and study more thoroughly the properties of the xc kernel for the homogeneous electron gas[1].

In this simple system $f_{\rm xc}^{\rm HEG}$ only depends on $\boldsymbol{r}-\boldsymbol{r}'$ and on $t-t'$, so it is convenient to work in Fourier space. Our knowledge of the function $f_{\rm xc}^{\rm HEG}(\boldsymbol{q},\omega)$ is quite limited. Several of its exact features can nevertheless be obtained through analytical manipulations. The zero frequency and zero momentum limit is given by

$$\lim_{\boldsymbol{q}\to 0} f_{\rm xc}^{\rm HEG}(\boldsymbol{q},\omega=0) = \frac{d^2}{dn^2}\left[n\epsilon_{\rm xc}^{\rm HEG}(n)\right] \equiv f_0(n)\,, \tag{74}$$

where $\epsilon_{\rm xc}^{\rm HEG}$, the xc energy per particle of the homogeneous electron gas, is known exactly from Monte-Carlo calculations[23]. Also the infinite frequency limit can be written as a simple expression

$$\begin{aligned}\lim_{\boldsymbol{q}\to 0} f_{\rm xc}^{\rm HEG}(\boldsymbol{q},\omega=\infty) &= -\frac{4}{5}n^{\frac{2}{3}}\frac{d}{dn}\left[\frac{\epsilon_{\rm xc}^{\rm HEG}(n)}{n^{2/3}}\right] + 6\,n^{\frac{1}{3}}\frac{d}{dn}\left[\frac{\epsilon_{\rm xc}^{\rm HEG}(n)}{n^{1/3}}\right] \\ &\equiv f_\infty(n)\,.\end{aligned} \tag{75}$$

From these two expression, one can prove that the zero frequency limit is always smaller than the infinite frequency limit, and that both these quantities are smaller than zero (according to the best approximations known for $E_{\rm xc}^{\rm HEG}$), i.e.

$$f_0(n) < f_\infty(n) < 0 \tag{76}$$

From the fact that $f_{\rm xc}$ is a real function when written in real space and in real time one can deduce the following symmetry relations

$$\begin{aligned}\Re f_{\rm xc}^{\rm HEG}(\boldsymbol{q},\omega) &= \Re f_{\rm xc}^{\rm HEG}(\boldsymbol{q},-\omega) \\ \Im f_{\rm xc}^{\rm HEG}(\boldsymbol{q},\omega) &= -\Im f_{\rm xc}^{\rm HEG}(\boldsymbol{q},-\omega)\,.\end{aligned} \tag{77}$$

From causality follow the Kramers-Kronig relations:

$$\begin{aligned}\Re f_{\rm xc}^{\rm HEG}(\boldsymbol{q},\omega) - f_{\rm xc}^{\rm HEG}(\boldsymbol{q},\infty) &= \mathcal{P}\int_{-\infty}^{\infty}\frac{d\omega'}{\pi}\frac{\Im f_{\rm xc}^{\rm HEG}(\boldsymbol{q},\omega)}{\omega-\omega'} \\ \Im f_{\rm xc}^{\rm HEG}(\boldsymbol{q},\omega) &= -\mathcal{P}\int_{-\infty}^{\infty}\frac{d\omega'}{\pi}\frac{\Re f_{\rm xc}^{\rm HEG}(\boldsymbol{q},\omega) - f_{\rm xc}^{\rm HEG}(\boldsymbol{q},\infty)}{\omega-\omega'}\,,\end{aligned} \tag{78}$$

where $\mathcal{P}$ denotes the principal value of the integral. Note that, as the infinite frequency limit of the xc kernel is different from zero, one has to subtract $f_{\rm xc}^{\rm HEG}(\boldsymbol{q},\infty)$ in order to apply the Kramers-Kronig relations.

Furthermore, by performing a perturbative expansion of the irreducible polarization to second order in e^2, one finds

$$\lim_{\omega\to\infty}\Im f_{\rm xc}^{\rm HEG}(\boldsymbol{q}=0,\omega) = -\frac{23\pi}{15\omega^{3/2}}\,. \tag{79}$$

The real part can be obtained with the help of the Kramers-Kronig relations

$$\lim_{\omega\to\infty}\Re f_{\rm xc}^{\rm HEG}(\boldsymbol{q}=0,\omega) = f_\infty(n) + \frac{23\pi}{15\omega^{3/2}}\,. \tag{80}$$

It is possible to write a analytical form for the long-wavelength limit of the imaginary part of $f_{\rm xc}$ that incorporates all these exact limits[24]

$$\Im f_{\rm xc}^{\rm HEG}(\boldsymbol{q}=0,\omega) \approx \frac{\alpha(n)\omega}{(1+\beta(n)\omega^2)^{\frac{5}{4}}}\,. \tag{81}$$

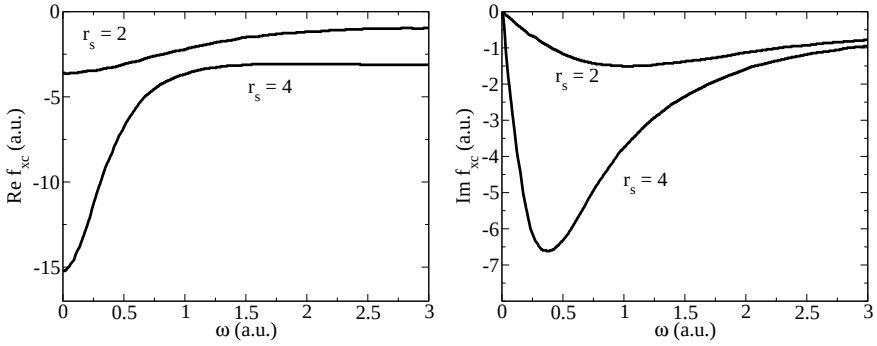

Fig. 1. Real and imaginary part of the parametrization for $f_{\rm xc}^{\rm HEG}$. Figure reproduced from Ref. [25].

The coefficients α and β are functions of the density, and can be determined uniquely by the zero and high frequency limits. A simple calculation yields

$$\alpha(n) = -A\left[f_\infty(n) - f_0(n)\right]^{\frac{5}{3}} \tag{82}$$

$$\beta(n) = B\left[f_\infty(n) - f_0(n)\right]^{\frac{4}{3}} , \tag{83}$$

where $A, B > 0$ and independent of n. Once again, by applying the Kramers-Kronig relations we can obtain the corresponding real part of $f_{\rm xc}^{\rm HEG}$

$$\begin{aligned}\Re f_{\rm xc}^{\rm HEG}(\boldsymbol{q}=0,\omega) = f_\infty + \frac{2\sqrt{2}\alpha}{\pi\sqrt{\beta}r^2}\left[2E\left(\frac{1}{\sqrt{2}}\right)\right. \\ \left. - \frac{1+r}{2}\Pi\left(\frac{1-r}{2},\frac{1}{\sqrt{2}}\right) - \frac{1-r}{2}\Pi\left(\frac{1+r}{2},\frac{1}{\sqrt{2}}\right)\right] ,\end{aligned} \tag{84}$$

where $r = \sqrt{1+\beta\omega^2}$ and E and Π are the elliptic integrals of second and third kind. In Fig. 1 we plot the real and imaginary part of $f_{\rm xc}^{\rm HEG}$ for two different densities ($r_{\rm s} = 2$ and $r_{\rm s} = 4$, where $r_{\rm s}$ is the Wigner-Seitz radius, $1/n = 4\pi r_{\rm s}^3/3$). The ALDA corresponds to approximating these curves by their zero frequency value. For very low frequencies, the ALDA is naturally a good approximation, but at higher frequencies it completely fails to reproduce the behavior of $f_{\rm xc}^{\rm HEG}$.

To understand how the ALDA can yield such good excitation energies, albeit exhibiting such a mediocre frequency dependence, we will look at a specific example, the process of photo-absorption by an atom. At low excitation frequencies, we expect the ALDA to work. As we increase the laser frequency, we start exciting deeper levels, promoting electrons from the inner shells of the atom to unoccupied states. The atomic density increases monotonically as we approach the nucleus. $f_{\rm xc}$ corresponding to that larger density (lower

r_s) has a much weaker frequency dependence, and is much better approximated by the ALDA than the low density curve. In short, by noticing that high frequencies are normally related to high densities, we realize that for practical applications the ALDA is often a reasonably good approximation. One should however keep in mind that these are simple heuristic arguments that may not hold in a real physical system.

4 Excitation energies

4.1 DFT techniques to calculate excitations

In this section we will present a short overview of the several techniques to calculate excitation energies that have appeared in the context of DFT over the past years. Indeed quite a lot of different approaches have been tried. Some are more or less *ad hoc*, others rely on a solid theoretical basis. Moreover, the degree of success varies considerably among the different techniques. The most successful of all is certainly TDDFT that has become the *de facto* standard for the calculation of excitations for finite systems. We will leave the discussion of excitation energies in TDDFT to the following sections, and concentrate for now on the "competitors". The first group of methods is based on a single determinant calculation, i.e. only one ground-state like calculation is performed, subject to the restriction that the Kohn-Sham occupation numbers are either 0 or 1.

As a first approximation to the excitation energies, one can simply take the differences between the ground-state Kohn-Sham eigenvalues. This procedure, although not entirely justifiable, is often used to get a rough idea of the excitation spectrum. We stress that the Kohn-Sham eigenvalues (as well as the Kohn-Sham wave-functions) *do not* have any physical interpretation. The exception is the eigenvalue of the highest occupied state that is equal to minus the ionization potential of the system[26].

The second scheme is based on the observation that the Hohenberg-Kohn theorem and the Kohn-Sham scheme can be formulated for the lowest state of each symmetry class[27]. In fact, the single modification to the standard proofs is to restrict the variational principle to wave-functions of a specific symmetry. The unrestricted variation will clearly yield the ground-state. The states belonging to different symmetry classes will correspond to excited states. The excitations can then be calculated by simple total-energy differences. This approach suffers from two serious drawbacks: i) Only the lowest lying excitation for each symmetry class is obtainable. ii) The xc functional that now enters the Kohn-Sham equations depends on the particular symmetry we have chosen. As specific approximations for a symmetry dependent xc functional are not available, one is relegated to use ground-state functionals. Unfortunately the excitation energies calculated in this way are only of moderate quality.

Another promising method was recently proposed by A. Görling[28]. The so-called generalized adiabatic connection Kohn-Sham formalism is no longer based on the Hohenberg-Kohn theorem but on generalized adiabatic connections associating a Kohn-Sham state with each state of the real system. This formalism was later extended to allow for the proper treatment of symmetry of the Kohn-Sham states[29]. The quality of the results obtained so far with this procedure varies: For alkali atoms the agreement with experimental excitation energies is quite good[28], but for the Carbon atom and the CO molecule the situation is considerably worse[29]. We note however that this method is still in its infancy, so further developments can be expected in the near future.

It is also possible to calculate excitation energies from the ground-state energy functional. In fact, it was proved by Perdew and Levy[30] that "every extremum density $n_i(\boldsymbol{r})$ of the ground-state energy functional $E_v[n]$ yields the energy E_i of a stationary state of the system." The problem is that not every excited-state density, $n_i(\boldsymbol{r})$, corresponds to an extremum of $E_v[n]$, which implies that not all excitation energies can be obtained from this procedure.

The last member of the first group of methods was proposed by Ziegler, Rauk and Baerends in 1977[31] and is based on an idea borrowed from multiconfiguration Hartree-Fock. The procedure starts with the construction of many-particle states with good symmetry, Ψ_i, by taking a finite superposition of states

$$\Psi_i = \sum_\alpha c_{i\alpha} \Phi_\alpha \,, \tag{85}$$

where Φ_α are Slater determinants of Kohn-Sham orbitals, and the coefficients $c_{i\alpha}$ are determined from group theory. Through a simple matrix inversion we can express the determinants as linear combinations of the many-body wavefunctions

$$\Phi_\beta = \sum_j a_{\beta j} \Psi_j \,. \tag{86}$$

By taking the expectation value of the Hamiltonian in the state Φ_β we arrive at

$$\langle \Phi_\beta | \, \hat{H} \, | \Phi_\beta \rangle = \sum_j |a_{\beta j}|^2 E_j \,, \tag{87}$$

where E_j is the energy of the many-body state Ψ_j. The "recipe" to calculate excitation energies is then: a) Build Φ_β from n Kohn-Sham orbitals (not necessarily the lowest); b) Make an ordinary Kohn-Sham calculation for each Φ_β, and associate the corresponding total energy E_β^{DFT} with $\langle \Phi_\beta | \, \hat{H} \, | \Phi_\beta \rangle$; c) Determine E_j by solving the system of linear equations, Eq. (87).

This methods works quite well in practice, and was frequently used in quantum chemistry till the advent of TDDFT. We should nevertheless indicate two of its limitations: i) The decomposition (85) is not unique and the system of linear equations can be under- or overdetermined. ii) The whole procedure of the "recipe" is not rigorously founded.

The next technique, the so-called ensemble DFT, makes use of fractional occupation numbers. Ensemble DFT, first proposed by Theophilou in 1979[32], evolves around the concept of an ensemble. In the simplest case it consists of a "mixture" of the ground state, Ψ_1, and the first excited state, Ψ_2, described by the density matrix[33–35]

$$\hat{D} = (1-\omega)\,|\Psi_1\rangle\,\langle\Psi_1| + \omega\;|\Psi_2\rangle\,\langle\Psi_2|\;, \tag{88}$$

where the weight, ω, is between 0 and 1/2 (in this last case the ensemble is called "equiensemble"). We can further define the ensemble energy and density

$$E(\omega) \;= (1-\omega)E_1 + \omega\; E_2 \tag{89}$$

$$n_\omega(\boldsymbol{r}) = (1-\omega)n_1(\boldsymbol{r}) + \omega\; n_2(\boldsymbol{r})\,. \tag{90}$$

At $\omega = 0$ the ensemble energy clearly reduces to the ground-state energy. Using the ensemble density it is possible to construct a DFT, i.e. to prove a Hohenberg-Kohn theorem and construct a Kohn-Sham scheme. The main features of the Kohn-Sham scheme are: i) The one-body orbitals have fractional occupations determined by the weight ω. ii) The xc functional depends on the weight, $E_{\rm xc}(\omega)$. To calculate the excitation energies from ensemble DFT we can follow two paths. The first involves obtaining the ground-state energy and the ensemble energy for some fixed ω, from which the excitation energy $E_1 - E_2$ trivially follows

$$E_2 - E_1 = \frac{E(\omega) - E(0)}{\omega}\,. \tag{91}$$

The second path is obtained by taking the derivative of Eq. (89)

$$\frac{dE(\omega)}{d\omega} = E_2 - E_1\,. \tag{92}$$

It is then possible to prove

$$E_2 - E_1 = \epsilon_\omega^{N+1} - \epsilon_\omega^{N} + \left.\frac{\partial E_{\rm xc}(\omega)}{\partial\omega}\right|_{n=n_\omega}\,. \tag{93}$$

Naturally, we need approximations to the xc energy functional, $E_{\rm xc}(\omega)$. An ensemble LDA was developed for the equiensemble by W. Kohn in 1986[36], by treating the ensemble as a reminiscent of a thermal ensemble. He then related $E_{\rm xc}(\omega)$ to the finite temperature xc energy of the homogeneous electron gas by equating the entropies of both systems. Unfortunately, the results obtained with this functional were not very encouraging. A promising approach, recently proposed, is the use of orbital functionals within an ensemble OEP method[37,38].

4.2 Full solution of the Kohn-Sham equations

One of the most important uses of TDDFT is the calculation of photo-absorption spectra. This problem can be solved in TDDFT either by propagating the time-dependent Kohn-Sham equations[39] or by using linear-response theory. In this section we will be concerned by the former, relegating the latter to the next section.

Let $\tilde{\varphi}_j(\boldsymbol{r})$ be the ground-state Kohn-Sham wave-functions for the system under study. We prepare the initial state for the time-dependent propagation by exciting the electrons with the electric field $v(\boldsymbol{r},t) = -k_0 x_\nu \delta(t)$, where $x_\nu = x, y, z$. The amplitude k_0 must be small in order to keep the response of the system linear and dipolar. Through this prescription *all* frequencies of the system are excited with equal weight. At $t = 0^+$ the initial state for the time evolution reads

$$\begin{aligned}\varphi_j(\boldsymbol{r}, t=0^+) &= \hat{T} \exp\left\{-\mathrm{i}\int_0^{0^+} dt\ \left[\hat{H}_{\mathrm{KS}} - k_0 x_\nu \delta(t)\right]\right\} \tilde{\varphi}_j(\boldsymbol{r}) \\ &= \exp\left[\mathrm{i}k_0 x_\nu\right] \tilde{\varphi}_j(\boldsymbol{r})\,. \end{aligned} \tag{94}$$

The Kohn-Sham orbitals are then further propagated during a finite time. The dynamical polarizability can be obtained from

$$\alpha_\nu(\omega) = -\frac{1}{k}\int d^3r\, x_\nu\, \delta n(\boldsymbol{r},\omega)\,. \tag{95}$$

In the last expression $\delta n(\boldsymbol{r},\omega)$ stands for the Fourier transform of $n(\boldsymbol{r},t) - \tilde{n}(\boldsymbol{r})$, where $\tilde{n}(\boldsymbol{r})$ is the ground-state density of the system. The quantity that is usually measured in experiments, the photo-absorption cross-section, is essentially proportional to the imaginary part of the dynamical polarizability averaged over the three spatial directions

$$\sigma(\omega) = \frac{4\pi\omega}{c}\frac{1}{3}\Im\sum_\nu \alpha_\nu(\omega)\,, \tag{96}$$

where c stands for the velocity of light. Although computationally more demanding than linear-response theory, this method is very flexible, and is easily extended to incorporate temperature effects, non-linear phenomena, etc. Note also that this approach only requires an approximation to the xc potential.

To illustrate the method, we present, in Fig. 2, the excitation spectrum of benzene calculated within the LDA/ALDA[3]. The agreement with experiment is quite remarkable, especially when looking at the $\pi \rightarrow \pi^*$ resonance at

[3] We will use the notation "A/B" consistently throughout the rest of this article to indicate that the ground-state xc potential used to calculate the initial state was "A", and that this state was propagated with the time-dependent xc potential "B". In the case of linear-response theory, "B" will denote the xc kernel.

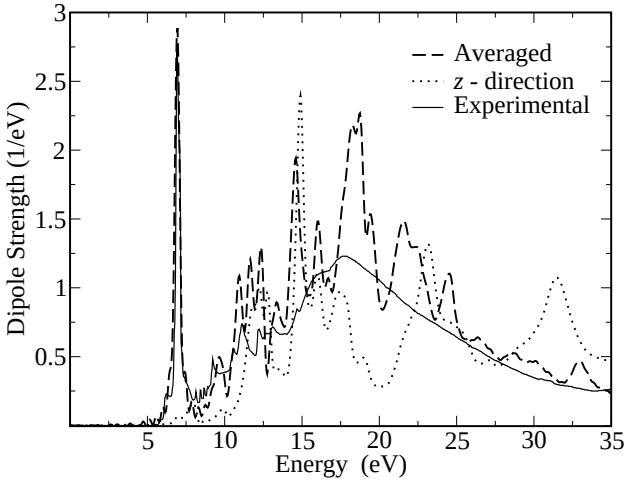

Fig. 2. Optical absorption of the benzene molecule. Experimental results from Ref. [40]. Figure reproduced from Ref. [41].

around 7 eV. The spurious peaks that appear in the calculation at higher energies are artifacts caused by an insufficient treatment of the unbound states. We furthermore observe that such good results are routinely obtained when applying the LDA/ALDA to several finite systems, from small molecules to metallic clusters and biological systems.

4.3 Excitations from linear-response theory

The first self-consistent solution of the linear response equation (69) was performed by Zangwill and Soven in 1980 using the LDA/ALDA [42]. Their results for the photo-absorption spectrum of Helium for energies just above the ionization threshold are shown in Fig. 3. Once more the theoretical curve compares very well to experiments.

Unfortunately, a full solution of Eq. (69) is still quite difficult numerically. Besides the large effort required to solve the integral equation, we need as an input the non-interacting response function. To obtain this quantity it is usually necessary to perform a summation over all states, both occupied and unoccupied [cf. Eq. (63)]. Such summations are sometimes slowly convergent and require the inclusion of many unoccupied states. There are however approximate frameworks that circumvent the solution of Eq. (69). The one we will present in the following was proposed by Petersilka *et al.* [22].

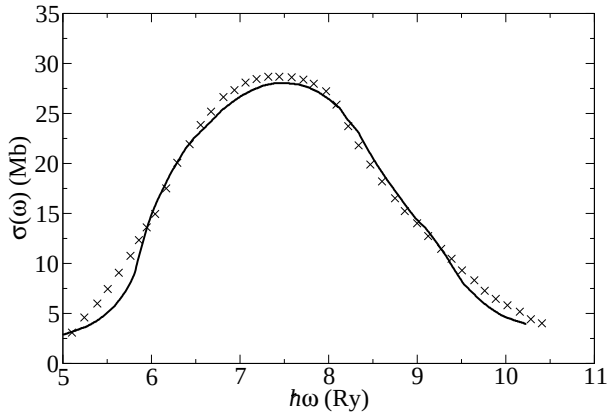

Fig. 3. Total photo-absorption cross-section of Xenon versus photon energy in the vicinity of the 4d threshold. The solid line represents TDDFT calculations and the crosses are the experimental results of Ref. [43]. Figure adapted from Ref. [42].

The density response function can be written in the Lehmann representation

$$\chi(\boldsymbol{r},\boldsymbol{r}',\omega) = \lim_{\eta\to 0^+} \sum_m \left[\frac{\langle 0|\,\hat\rho(\boldsymbol{r})\,|m\rangle\,\langle m|\,\hat\rho(\boldsymbol{r}')\,|0\rangle}{\omega-(E_m-E_0)+\mathrm{i}\eta} - \frac{\langle 0|\,\hat\rho(\boldsymbol{r}')\,|m\rangle\,\langle m|\,\hat\rho(\boldsymbol{r})\,|0\rangle}{\omega+(E_m-E_0)+\mathrm{i}\eta} \right], \tag{97}$$

where $|m\rangle$ is a complete set of many-body states with energies E_m. From this expansion it is clear that the full response function has poles at frequencies that correspond to the excitation energies of the interacting system

$$\Omega = E_m - E_0\,. \tag{98}$$

As the external potential does not have any special pole structure as a function of ω, Eq. (61) implies that also $n^{(1)}(\boldsymbol{r},\omega)$ has poles at the excitation energies, Ω. On the other hand, $\chi_{\rm KS}$ has poles at the excitation energies of the non-interacting system, i.e. at the Kohn-Sham orbital energy differences $\epsilon_j - \epsilon_k$ [cf. Eq. (63)].

By rearranging the terms in Eq. (68) we obtain the fairly suggestive equation

$$\int d^3r'\,\left[\delta(\boldsymbol{r}-\boldsymbol{r}') - \Xi(\boldsymbol{r},\boldsymbol{r}',\omega)\right] n^{(1)}(\boldsymbol{r}',\omega) = \int d^3r'\,\chi_{\rm KS}(\boldsymbol{r},\boldsymbol{r}',\omega) v^{(1)}(\boldsymbol{r}',\omega) \tag{99}$$

where the function Ξ is defined by

$$\Xi(\boldsymbol{r},\boldsymbol{r}',\omega) = \int d^3r''\,\chi_{\rm KS}(\boldsymbol{r},\boldsymbol{r}'',\omega)\left[\frac{1}{|\boldsymbol{r}''-\boldsymbol{r}'|} + f_{\rm xc}(\boldsymbol{r}'',\boldsymbol{r}',\omega)\right] \tag{100}$$

As noted previously, in the limit $\omega \to \Omega$ the linear density $n^{(1)}$ has a pole, while the right-hand side of Eq. (100) remains finite. For the equality (100) to hold, it is therefore required that Ξ has zero eigenvalues at the excitation energies Ω, i.e. $\lambda(\omega) \to 1$ when $\omega \to \Omega$, where $\lambda(\omega)$ is the solution of the eigenvalue equation

$$\int d^3\boldsymbol{r}'\, \Xi(\boldsymbol{r},\boldsymbol{r}',\omega)\xi(\boldsymbol{r}',\omega) = \lambda(\omega)\xi(\boldsymbol{r},\omega)\,. \tag{101}$$

This is a rigorous statement, that allows the determination of the excitation energies of the systems from the knowledge of $\chi_{\rm KS}$ and $f_{\rm xc}$. It is possible to transform this equation into another eigenvalue equation having the true excitation energies of the system, Ω, as eigenvalues[44]. We start by defining the quantity

$$\zeta_{jk}(\omega) = \int d^3r' \int d^3r''\, \varphi_j^*(\boldsymbol{r}'')\varphi_k(\boldsymbol{r}'') \left[\frac{1}{|\boldsymbol{r}''-\boldsymbol{r}'|} + f_{\rm xc}(\boldsymbol{r}'',\boldsymbol{r}',\omega)\right] \xi(\boldsymbol{r}',\omega)\,. \tag{102}$$

With the help of ζ_{jk} Eq. (101) can be rewritten in the form

$$\sum_{jk} \frac{(f_k - f_j)\,\varphi_j(\boldsymbol{r})\varphi_k^*(\boldsymbol{r})}{\omega - (\epsilon_j - \epsilon_k) + i\eta}\zeta_{jk}(\omega) = \lambda(\omega)\xi(\boldsymbol{r},\omega)\,. \tag{103}$$

By solving this equation for $\xi(\boldsymbol{r},\omega)$ and inserting the result into Eq. (102), we arrive at

$$\sum_{j'k'} \frac{M_{jk,j'k'}}{\omega - (\epsilon_{j'} - \epsilon_{k'}) + i\eta}\zeta_{j'k'}(\omega) = \lambda(\omega)\zeta_{jk}(\omega) \tag{104}$$

where we have defined the matrix element

$$M_{jk,j'k'}(\omega) = (f_{k'} - f_{j'}) \int d^3r \int d^3r'\, \varphi_j^*(\boldsymbol{r})\varphi_k(\boldsymbol{r})\varphi_j(\boldsymbol{r}')\varphi_k^*(\boldsymbol{r}') \times \left[\frac{1}{|\boldsymbol{r}-\boldsymbol{r}'|} + f_{\rm xc}(\boldsymbol{r},\boldsymbol{r}',\omega)\right]\,. \tag{105}$$

Introducing the new eigenvector

$$\beta_{jk} = \frac{\zeta_{jk}(\Omega)}{\Omega - (\epsilon_{j'} - \epsilon_{k'})}\,, \tag{106}$$

taking the $\eta \to 0$ limit, and by using the condition $\lambda(\Omega) = 1$, it is straightforward to recast Eq. (104) into the eigenvalue equation

$$\sum_{j'k'} \left[\delta_{jj'}\delta_{kk'}(\epsilon_{j'} - \epsilon_{k'}) + M_{jk,j'k'}(\Omega)\right]\beta_{j'k'} = \Omega\beta_{jk}\,. \tag{107}$$

It is also possible to derive an operator whose eigenvalues are the *square* of the true excitation energies, thereby reducing the dimension of the matrix equation (107)[45]. The oscillator strengths can be obtained from the eigenfunctions of the operator.

The eigenvalue equation, Eq. (107), can be solved in several different ways. For example, it is possible to expand all quantities in a suitable basis and solve numerically the resulting matrix-eigenvalue equation. As an alternative, we can perform a Laurent expansion of the response function around the excitation energy

$$\chi_{\rm KS}(\boldsymbol{r},\boldsymbol{r}',\omega) = \lim_{\eta\to 0^+} \frac{\varphi_{j_0}(\boldsymbol{r})\varphi^*_{j_0}(\boldsymbol{r}')\varphi_{k_0}(\boldsymbol{r}')\varphi^*_{k_0}(\boldsymbol{r})}{\omega - (\epsilon_{j_0}-\epsilon_{k_0}) + i\eta} + \text{higher order}\,. \tag{108}$$

By neglecting the higher-order terms, a simple manipulation of Eq. (101) yields the so-called single-pole approximation (SPA) to the excitation energies

$$\Omega = \Delta\epsilon + K(\Delta\epsilon)\,, \tag{109}$$

where $\Delta\epsilon$ is the difference between the Kohn-Sham eigenvalue of the unoccupied orbital j_0 and the occupied orbital k_0,

$$\Delta\epsilon = \epsilon_{j_0} - \epsilon_{k_0} \tag{110}$$

and K is a correction given by

$$K(\Delta\epsilon) = 2\Re \int d^3r \int d^3r'\, \varphi_{j_0}(\boldsymbol{r})\varphi^*_{j_0}(\boldsymbol{r}')\varphi_{k_0}(\boldsymbol{r}')\varphi^*_{k_0}(\boldsymbol{r}) \times \left[\frac{1}{|\boldsymbol{r}-\boldsymbol{r}'|} + f_{\rm xc}(\boldsymbol{r},\boldsymbol{r}',\Delta\epsilon)\right]. \tag{111}$$

Although not as precise as the direct solution of the eigenvalue equation, Eq. (107), this formula provides us with a simple and fast way to calculate the excitation energies.

To assert how well this approach works in practice we list, in Tab. 1, the $^1\mathrm{S} \rightarrow {}^1\mathrm{P}$ excitation energies for several atoms[22]. Surprisingly perhaps, the eigenvalue differences, $\Delta\epsilon$, are already of the proper order of magnitude. For other systems they can be even much closer (cf. Tab. 3). Adding the correction K then brings the numbers indeed very close to experiments for both xc functionals tried. We furthermore notice that the EXX/PGG functional gives clearly superior results than the LDA/ALDA. This is related to the different quality of the unoccupied states generated with the two ground-state xc functionals. The unoccupied states typically probe the farthest regions from the system, where the LDA potential exhibits severe deficiencies (as previously mentioned in section 2.4). As the EXX potential does not suffer from this problem, it yields better unoccupied orbitals and consequently better excitation energies.

Atom	$\Delta\epsilon_{\rm LDA}$	$\Omega_{\rm LDA/ALDA}$	$\Delta\epsilon_{\rm EXX}$	$\Omega_{\rm EXX/PGG}$	Ωexp
Be	0.129	0.200	0.130	0.196	0.194
Mg	0.125	0.176	0.117	0.164	0.160
Ca	0.088	0.132	0.079	0.117	0.108
Zn	0.176	0.239	0.157	0.211	0.213
Sr	0.082	0.121	0.071	0.105	0.099
Cd	0.152	0.214	0.135	0.188	0.199

Table 1. ^{1}S $\rightarrow$ ^{1}P excitation energies for selected atoms. $\Omega_{\rm exp}$ denotes the experimental results from [46]. All energies are in Hartrees. Table adapted from Ref. [22].

In Tab. 2 we show the excitation energies of the CO molecule. This case is slightly more complicated than the previous example due to the existence of degeneracies in the eigenspectrum of the CO molecule. Although the Kohn-Sham eigenvalue differences are equal for all transitions involving degenerate states, the true excitation energies depend on the symmetry of the initial and final many-body states. As is clearly seen from the table, this splitting of the excitations is correctly described by the correction factor, K.

State		$\Delta\epsilon_{\rm LDA}$	$\Omega^{\rm SPA}_{\rm LDA/ALDA}$	$\Omega^{\rm full}_{\rm LDA/ALDA}$	exp.
A $^1\Pi$	$5\sigma \rightarrow 2\pi$	0.2523	0.3268	0.3102	0.3127
a $^3\Pi$			0.2238	0.2214	0.2323
B $^1\Sigma^+$	$5\sigma \rightarrow 6\sigma$	0.3332	0.3389	0.3380	0.3962
b $^3\Sigma^+$			0.3315	0.3316	0.3822
I $^1\Sigma^-$			0.3626	0.3626	0.3631
e $^3\Sigma^-$			0.3626	0.3626	0.3631
a' $^3\Sigma^+$	$1\pi \rightarrow 2\pi$	0.3626	0.3181	0.3149	0.3127
D $^1\Delta$			0.3812	0.3807	0.3759
d $^3\Delta$			0.3404	0.3396	0.3440
c $^3\Pi$	$4\sigma \rightarrow 2\pi$	0.4388	0.4204	0.4202	0.4245
E $^1\Pi$	$1\pi \rightarrow 6\sigma$	0.4436	0.4435	0.4435	0.4237

Table 2. Excitation energies for the CO molecule. $\Omega^{\rm SPA}_{\rm LDA/ALDA}$ are the LDA/ALDA excitation energies obtained from Eq. (109), and $\Omega^{\rm SPA}_{\rm LDA/ALDA}$ are obtained from the solution of Eq. (107) neglecting continuum states. "exp" are the experimental results from Ref. [47]. All energies are in Hartrees. Table reproduced from Ref. [48].

We remember that several approximations have been made to produce the previous results. First a static Kohn-Sham calculation was performed with an approximate $v_{\rm xc}$. Then the resulting eigenfunctions and eigenvalues were used in Eq. (109) to obtain the excitation energies. In the last step, we used an approximate form for the xc kernel, $f_{\rm xc}$, and we neglected the higher order terms in the Laurent expansion of the response functions. To assert which of

these approximations is more important, we can look at the lowest excitation energies of the He atom. For this simple system the *exact* stationary Kohn-Sham potential is known[49], so we can eliminate the first source of error. We can then test different approximations for $f_{\rm xc}$, both by performing the single-pole approximation or not. The results are summarized in Tab. 3. We first note that the quality of the results is almost insensitive to the xc kernel used. Both using the ALDA or the PGG yield the same mean error. This statement seems to hold not only for atoms but also to molecular systems[50]. From the table it is also clear that the SPA is an excellent approximation and that the calculated excitation energies are in very close agreement to the exact values. Why, and under which circumstances this is the case is discussed in detail in Refs. [51,52]. This leads us to conclude that the crucial approximation to obtain excitation energies in TDDFT is the choice of the static xc potential used to calculate the Kohn-Sham eigenfunctions and eigenvalues.

			exact/ALDA (xc)		exact/PGG		
State	$k_0 \to j_0$	$\Delta\epsilon_{\rm KS}$	SPA	full	SPA	full	exact
2^3S	$1s \to 2s$	0.7460	0.7357	0.7351	0.7232	0.7207	0.7285
2^1S			0.7718	0.7678	0.7687	0.7659	0.7578
3^3S	$1s \to 3s$	0.8392	0.8366	0.8368	0.8337	0.8343	0.8350
3^1S			0.8458	0.8461	0.8448	0.8450	0.8425
4^3S	$1s \to 4s$	0.8688	0.8678	0.8679	0.8667	0.8671	0.8672
4^1S			0.8714	0.8719	0.8710	0.8713	0.8701
2^3P	$1s \to 2p$	0.7772	0.7702	0.7698	0.7693	0.7688	0.7706
2^1P			0.7764	0.7764	0.7850	0.7844	0.7799
3^3P	$1s \to 3s$	0.8476	0.8456	0.8457	0.8453	0.8453	0.8456
3^1P			0.8483	0.8483	0.8500	0.8501	0.8486
4^3P	$1s \to 4s$	0.8722	0.8714	0.8715	0.8712	0.8713	0.8714
4^1P			0.8726	0.8726	0.8732	0.8733	0.8727
Mean abs. dev.			0.0011	0.0010	0.0010	0.0010	
Mean % error			0.15%	0.13%	0.13%	0.13%	

Table 3. Comparison of the excitation energies of neutral Helium, calculated from the exact xc potential[49] by using approximate xc kernels. SPA stands for "single pole approximations", while "full" means the complete solution of Eq. (107). The exact values are from a non-relativistic variational calculation[53]. The mean absolute deviation and mean percentage errors also include the transitions from the 1s until the 9s and 9p states. All energies are in Hartrees. Table adapted from Ref. [17].

4.4 When does it not work?

In the previous sections we showed the results of several TDDFT calculations, most of them agreeing quite well with experiment. Clearly no physical

theory works for all systems and situations, and TDDFT is not an exception. It is the purpose of this section to show some examples where the theory does not work. However, before proceeding with our task, we should specify what we mean by "failures of TDDFT". TDDFT is an *exact* reformulation of the time-dependent many-body Schrödinger equation – it can only fail in situations where quantum-mechanics also fails. The key approximation made in practical applications is the approximation for the xc potential. Errors in the calculations should therefore be imputed to the functional used. As a large majority of TDDFT calculations use the ALDA or the adiabatic GGA, we will be mainly interested in the errors caused by these approximate functional. Furthermore, and as we already mentioned in the previous section, there are usually two sources for the errors in the calculation: i) The functional used to obtain the Kohn-Sham ground-state; ii) The approximate time-dependent xc potential. In any discussion on the errors of TDDFT the effects of these two sources have to be clearly separated. With these arguments in mind let us then proceed.

Our first example is the calculation of optical properties of long conjugated molecular chains[54]. Using the local or gradient-corrected approximations can give overestimations of several orders of magnitude. The problem is related to a non-local dependence of the xc potential: In a system with an applied electric field, the exact xc potential develops a linear part that counteracts the applied field[54,55]. This term is completely absent in both the LDA and the GGA, but is present in more non-local functionals like the EXX.

A related problem occurs in solids[56]. In fact, TDLDA does not work properly for the calculation of excitations of non-metallic solids, especially in systems like wide-band gap semiconductors. For infinite systems, the Coulomb potential is (in momentum space) $4\pi/q^2$. It is then clear from the response equation (69) that if $f_{\rm xc}$ is to correct the non-interacting response for $q \to 0$ it will have to contain a term that behaves asymptotically as $1/q^2$ when $q \to 0$. This is not the case for the local or gradient-corrected approximations. Several attempts have been done to correct this problem from which we mention Refs. [57–60].

As other faults of the TDLDA we can mention the incorrect excitation energies of the stretched H_2 molecule[61], the large error in the calculation of singlet-triplet separation energies[62], the underestimate of the onset of absorption for some clusters[50], etc. Despite these failures, we would like to emphasize that TDLDA does work very well for the calculation of excitations in a large class of systems.

5 Atoms and molecules in strong laser fields

5.1 What is a "strong" laser?

Before discussing the behavior of atoms and molecules in strong laser fields, we have to specify what the adjective "strong" means in this context. The electric field that an electron feels in a Hydrogen atom, at the distance of one Bohr from the nucleus, is

$$E = \frac{1}{4\pi\epsilon_0}\frac{e}{a_0^2} = 5.1 \times 10^9\,\mathrm{V/m}\,. \tag{112}$$

The laser intensity that corresponds to this field is given by

$$I = \frac{1}{2}\epsilon_0 c E^2 = 3.51 \times 10^{16}\,\mathrm{W/cm^2}\,. \tag{113}$$

We can clearly consider a laser to be "strong" when its intensity becomes comparable to (113). In this regime, perturbation theory is no longer applicable, and the theorist has to resort to non-perturbative methods. When approaching these high intensities, a wealth of non-linear phenomena appear, like multi-photon ionization, above threshold ionization (ATI), high harmonic generation, etc.

The fact that allowed systematic investigation of these high-intensity phenomena was the remarkable evolution in laser technology during the past four decades. Through a series of technological breakthroughs, scientists were able to boost the peak intensity of pulsed lasers from $10^9\,\mathrm{W/cm^2}$ in the 1960s, to more than $10^{21}\,\mathrm{W/cm^2}$ of the current systems – 12 orders of magnitude! Besides this increase in laser intensity, very short pulses – sometimes of the order of hundreds of attoseconds ($1\,\mathrm{as} = 10^{-18}\,\mathrm{s}$) – became available at ultraviolet or soft X-ray frequencies [63,64]. In the present context we are concerned mainly with intensities in the range $10^{13} - 10^{16}\,\mathrm{W/cm^2}$. For higher intensities many-body effects associated with the electron-electron interaction – which are the main interest of DFT – become less and less important due to the strongly dominant external field.

TDDFT is a tool particularly suited for the study of systems under the influence of strong lasers. We recall that the time-dependent Kohn-Sham equations yield the *exact* density of the system, including *all* non-linear effects. To simulate laser induced phenomena it is customary to start from the ground-state of the system, which is then propagated under the influence of the potential

$$v_{\mathrm{TD}}(\boldsymbol{r}, t) = E f(t) z \sin(\omega t)\,. \tag{114}$$

v_{TD} describes a laser of frequency ω and amplitude E[4]. The function $f(t)$, typically a Gaussian or the square of a sinus, defines the temporal shape

[4] The amplitude is related to the laser intensity by the relation $I = \frac{1}{2}\epsilon_0 c E^2$.

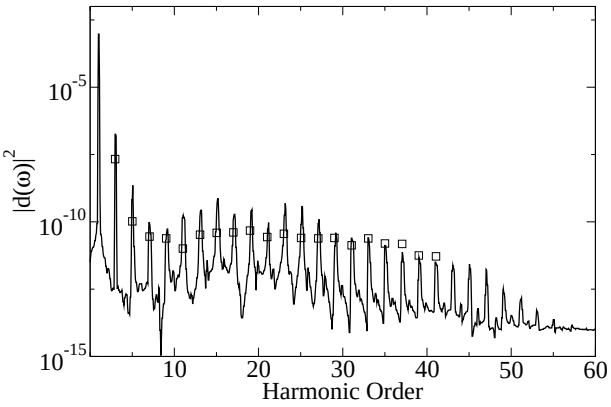

Fig. 4. Harmonic spectrum for He at $\lambda = 616\,\mathrm{nm}$ and $I = 3.5 \times 10^{14}\,\mathrm{W/cm^2}$. The squares represent experimental data taken from Ref. [65] normalized to the value of the 33rd harmonic of the calculated spectrum. Figure reproduced from Ref. [66].

of the laser pulse. From the time-dependent density it is then possible to calculate the photon spectrum using the relation

$$\sigma(\omega) \propto |d(\omega)|^2 \,, \tag{115}$$

where $d(\omega)$ is the Fourier transform of the time-dependent dipole of the system

$$d(\omega) = \int d^3r\, z\, n(\boldsymbol{r}, t)\,. \tag{116}$$

Other observables, such as the total ionization yield or the ATI spectrum, are much harder to calculate within TDDFT. Even though these observables (as all others) are functionals of the density by virtue of the Runge-Gross theorem, the explicit functional dependence is unknown and has to be approximated.

5.2 High-harmonic generation

If we shine a high-intensity laser onto an atom (or a molecule, or even a surface), an electron may absorb several photons and then return to its ground-state by emitting a single photon. The photon will have a frequency which is an integer multiple of the external laser frequency. This process, known as high-harmonic generation, has received a great deal of attention from both theorists and experimentalists. As the outgoing high-energy photons maintain a fairly high coherence, they can be used as a source for X-ray lasers.

A typical high-harmonic spectrum is shown in Fig. 4 for the Helium atom. The squares represent experimental data taken from Ref. [65], and the solid

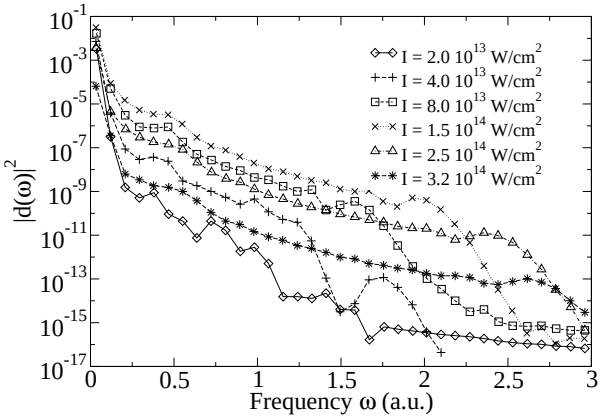

Fig. 5. Harmonic spectra of Hydrogen at a laser wavelength of $\lambda = 1064\,\text{nm}$ for various laser intensities. Figure reproduced from Ref. [67].

line was obtained from a calculation using the EXX/EXX functional[66]. The spectrum consists of a series of peaks, first decreasing in amplitude and then reaching a plateau that extends to very high frequency. The peaks are placed at the odd multiples of the external laser frequency (the even multiples are dipole forbidden by symmetry). We note that any approach based on perturbation theory would yield a harmonic spectrum that decays exponentially, i.e. such a theory could never reproduce the measured peak intensities. TDDFT, on the other hand, gives a quite satisfactory agreement with experiment.

As mentioned before, high-harmonics can be used as a source of soft X-ray lasers. For such purpose, one tries to optimize the laser parameters, the frequency, intensity, etc., in order to increase the intensity of the emitted harmonics, and to extend the plateau the farthest possible. By performing "virtual experiments", TDDFT can be once more used to tackle such important problem. As an illustration, we show, in Fig. 5, the result of irradiating a Hydrogen atom with lasers of the same frequency but with different intensities. For clarity, we only show the position of the peaks, and the points were connected by straight lines. As we increase the intensity of the laser, the amplitude of the harmonics also increases, until reaching a maximum at $I = 1.5 \times 10^{14}\,\text{W/cm}^2$. A further increase of the intensity will, however, decrease the produced harmonics. This reflects the two competing processes that happen upon multiple absorption of photons: The electron can either ionize, or fall back into the ground-state emitting a highly energetic photon. Beyond a certain threshold intensity the ionization channel begins to predominate, thereby reducing the production of harmonics. Other laser parameters, like the intensity, or the spectral composition of the laser, are also found to influence the generation of high-harmonics in atoms[66,67].

5.3 Multi-photon ionization

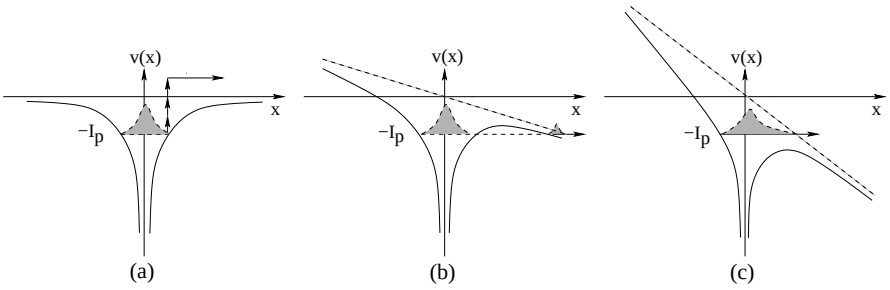

Fig. 6. Ionization in strong laser fields: (a) Multi-photon ionization; (b) Tunneling; (c) Over the barrier.

To better understand the process of ionization of an atom in strong laser fields, it is convenient to resort to a simple quasi-static picture. In Fig. 6 we have depicted a one-electron atom at a time t after the beginning of the laser pulse. The dashed line represents the laser potential felt by the electron and the solid line the total (i.e. the nuclear plus the laser) potential. Three different regimes of ionizations are governed by the Keldish parameter,

$$\gamma = \frac{\omega}{E}\,. \tag{117}$$

At low intensities ($I < 10^{14}\,\mathrm{W/cm^2}$, $\gamma \gg 1$) the electron has to absorb several photons before leaving the atom. This is the so-called multi-photon ionization regime. At higher intensities ($I \leq 10^{15}\,\mathrm{W/cm^2}$, $\gamma \approx 1$) we enter the tunneling regime. If we further increase the strength of the laser field ($I > 10^{16}\,\mathrm{W/cm^2}$, $\gamma \ll 1$), then the electron can simply pass over the barrier.

The measured energy spectrum of the outgoing photo-electrons is called the above threshold ionization (ATI) spectrum[68]. As the electron can absorb more photons than the necessary to escape the atom, an ATI spectrum will consist of a sequence of equally spaced peaks at energies

$$E = (n+s)\omega - I_\mathrm{p} \tag{118}$$

where n is a natural integer, s is the minimum integer such that $s\,\omega - I_\mathrm{p} > 0$, and I_p denotes the ionization potential of the system.

Another interesting observable is the number of outgoing charged atoms as a function of the laser intensity. The two sets of points in Fig. 7 represent the yield of singly ionized and doubly ionized Helium. The solid curve on the right is the result of a calculation assuming a sequential mechanism for the double ionization of Helium, i.e., the He^{2+} is generated by first removing one electron from He, and then a second from He^{+}. Strikingly, this

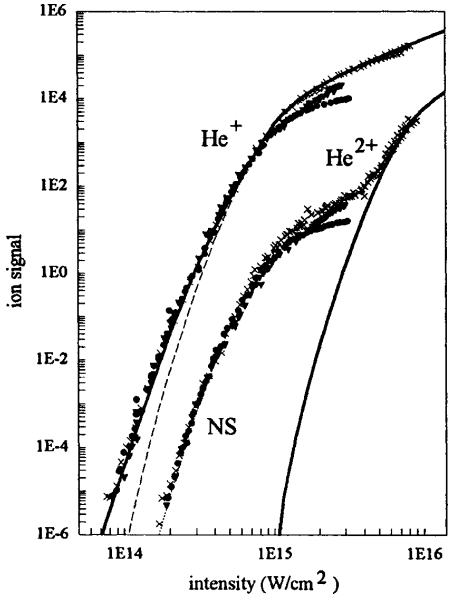

Fig. 7. Measured He^+ and He^{2+} yields as a function of the laser intensity. The solid curve on the right is the calculated sequential He^{2+} yield. Figure reproduced from Ref. [69].

naïve sequential mechanism is wrong by six orders of magnitude for some intensities.

Similar experimental results were found for a variety of molecules. Furthermore, in these more complex systems, the coupling of the nuclear and the electronic degrees of freedom gives rise to new physical phenomena. As an illustrative example of such phenomena, we refer the so-called ionization induced Coulomb explosion[70].

5.4 Ionization yields from TDDFT

It is apparent from Fig. 7 that a simple sequential mechanism is insufficient to describe the double ionization of Helium. In this section we will show how one can try to go beyond this simple picture with the use of TDDFT[71].

To calculate the Helium yields we invoke a geometrical picture of ionization. We divide the three-dimensional space, $\mathbb{R}^3$, into a (large) box, A, containing the Helium atom, and its complement, $B = \mathbb{R}^3 \backslash A$. Normalization of the (two-body) wave function of the Helium atom, $\Psi(\boldsymbol{r}_1, \boldsymbol{r}_2, t)$, then implies

$$1 = \int_A\int_A d^3r_1 d^2r_2 \left|\Psi(\boldsymbol{r}_1, \boldsymbol{r}_2, t)\right|^2 + 2\int_A\int_B d^3r_1 d^2r_2 \left|\Psi(\boldsymbol{r}_1, \boldsymbol{r}_2, t)\right|^2 \quad (119)$$

$$+\int_B\int_B d^3r_1 d^2r_2\,|\Psi(\boldsymbol{r}_1,\boldsymbol{r}_2,t)|^2\;,$$

where the subscript "X" has the meaning that the space integral is only over region X. A long time after the end of the laser excitation, we expect that all ionized electrons are in region B. This implies that the first term in the right-hand side of Eq. (119) measures the probability that an electron remains close to the nucleus; Similarly, the second term is equal to the probability of finding an electron in region A and simultaneously another electron far from the nucleus, in region B. This is interpreted as single ionization; Likewise, the final term is interpreted as the probability for double ionization. Accordingly, we will refer to these terms as $p^{(0)}(t)$, $p^{(+1)}(t)$, and $p^{(+2)}(t)$.

To this point of the derivation we have utilized the many-body wavefunction to define the ionization probabilities. Our goal is however to construct a density functional. For that purpose we introduce the pair-correlation function

$$g[n](\boldsymbol{r}_1,\boldsymbol{r}_2,t)=\frac{2\,|\Psi(\boldsymbol{r}_1,\boldsymbol{r}_2,t)|^2}{n(\boldsymbol{r}_1,t)n(\boldsymbol{r}_2,t)} \tag{120}$$

and rewrite

$$\begin{aligned}
p^{(0)}(t) &= \frac{1}{2}\int_A\int_A d^3r_1 d^3r_2\; n(\boldsymbol{r}_1,t)n(\boldsymbol{r}_2,t)g[n](\boldsymbol{r}_1,\boldsymbol{r}_2,t)\\
p^{(+1)}(t) &= \int_A d^3r\; n(\boldsymbol{r},t) - 2p^{(0)}(t)\\
p^{(+2)}(t) &= 1-p^{(0)}(t)-p^{(+1)}(t)\,.
\end{aligned} \tag{121}$$

We recall that by virtue of the Runge-Gross theorem g is a functional of the time-dependent density. Separating g into an exchange part (which is simply $1/2$ for a two electron system) and a correlation part,

$$g[n](\boldsymbol{r}_1,\boldsymbol{r}_2,t)=\frac{1}{2}+g_c[n](\boldsymbol{r}_1,\boldsymbol{r}_2,t) \tag{122}$$

we can cast Eq. (121) into the form

$$\begin{aligned}
p^{(0)}(t) &= [N_{1\mathrm{s}}(t)]^2+K(t)\\
p^{(+1)}(t) &= 2N_{1\mathrm{s}}(t)\,[1-N_{1\mathrm{s}}(t)]-2K(t)\\
p^{(+2)}(t) &= [1-N_{1\mathrm{s}}(t)]^2+K(t)
\end{aligned} \tag{123}$$

with the definitions

$$N_{1\mathrm{s}}(t)=\frac{1}{2}\int_A d^3r\; n(\boldsymbol{r},t)=\int_A d^3r\;\;|\varphi_{1\mathrm{s}}(\boldsymbol{r},t)|^2 \tag{124}$$

$$K(t) = \frac{1}{2}\int_A\int_A d^3r_1 d^3r_2\; n(\boldsymbol{r}_1,t)n(\boldsymbol{r}_2,t)g_c[n](\boldsymbol{r}_1,\boldsymbol{r}_2,t)\,. \tag{125}$$

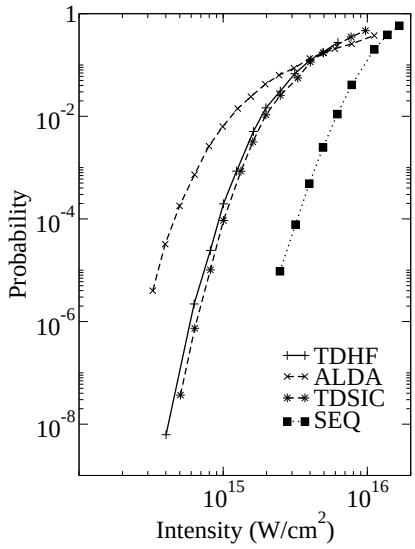

Fig. 8. Calculated double-ionization probabilities from the ground-state of Helium irradiated by a 16 fs, 780 nm laser pulse for different choices of the time-dependent xc potentials. Figure reproduced from Ref. [71].

In Fig. 8 we depict the probability for double ionization of Helium calculated from Eq. (123) by neglecting the correlation part of g. It is clear that all functionals tested yield a significant improvement over the simple sequential model. Due to the incorrect asymptotic behavior of the ALDA potential, the ALDA overestimates ionization: The outermost electron of Helium is not sufficiently bound and ionizes too easily.

To compare the TDDFT results with experiment it is preferable to look at the ratio of double- to single-ionization yields. This simple procedure eliminates the experimental error in determining the absolute yields. Clearly all TDDFT results presented in Fig. 9 are of very low quality, sometimes wrong by two orders of magnitude. We note that *two* approximations are involved in the calculation: The time-dependent xc potential used to propagate the Kohn-Sham equations, and the neglect of the correlation part of the pair-correlation function. By using a one-dimensional Helium model, Lappas and van Leeuwen were able to prove that even the simplest approximation for g was able to reproduce the knee structure[72]. As neither of the TDDFT calculations depicted in Fig. 9 show the knee structure, it seems that the approximation for the time-dependent xc potential is the most important in obtaining the ionization yields.

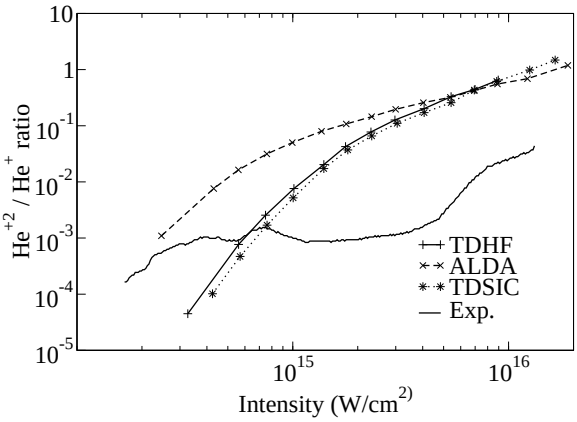

Fig. 9. Comparison of the ratios of double- to single-ionization probability calculated for different choices of the time-dependent xc potential. Figure reproduced from Ref. [71].

6 Conclusion

In this chapter we tried to give a brief, yet pedagogical overview of TDDFT, from its mathematical foundations – the Runge-Gross theorem and the time-dependent Kohn-Sham scheme – to some of its applications, both in the linear and in the non-linear regimes. In the linear regime, TDDFT has become the standard tool to calculate excitation energies within DFT, and is now incorporated into the major quantum-chemistry codes. In the non-linear regime, TDDFT is able to describe extremely non-linear effects, like high-harmonic generation, or multi-photon ionization. Unfortunately, some problems, like the knee structure in the yield of doubly ionized Helium, are still beyond the reach of modern time-dependent xc potentials. In our opinion, we should not dismiss these problems as failures of TDDFT, but as a challenge to the next generation of "density-functionalists", in their quest for better approximations to the elusive xc potential.

Acknowledgments

We would like to thank L. Wirtz and A. Rubio for their useful suggestions and comments, and also to A. Castro for his invaluable help in producing the figures.

References

1. E. K. U. Gross and W. Kohn, Adv. Quantum Chem. **21**, 255 (1990).

2. E. K. U. Gross, J. F. Dobson, and M. Petersilka, in *Topics in Current Chemistry*, edited by R. F. Nalewajski (Springer Verlag, Heidelberg, 1996), Vol. 181, p. 81.
3. G. Onida, L. Reinig, and A. Rubio, Rev. Mod. Phys. **74**, 601 (2002).
4. N. T. Maitra *et al.*, in *Reviews in Modern Quantum Chemistry: A Celebration of the Contributions of R. G. Parr*, edited by K. D. Sen (World Scientific, Singapore, 2002).
5. E. Runge and E. K. U. Gross, Phys. Rev. Lett. **52**, 997 (1984).
6. P. Hohenberg and W. Kohn, Phys. Rev. **136**, B864 (1964).
7. W. Kohn and L. J. Sham, Phys. Rev. **140**, A1133 (1965).
8. Dundas, Taylor, Parker, and J. Smyth, J. Phys. B **32**, L231 (1999).
9. S. Chelkowsky, T. Zuo, O. Atabek, and A. D. Brandrauk, Phys. Rev. A **52**, 2977 (1995).
10. T. Zuo and A. D. Bandrauk, Phys. Rev. A **54**, 3254 (1996).
11. E. K. U. Gross, C. A. Ullrich, and U. J. Gossman, in *Density Functional Theory*, Vol. 337 of *NATO ASI, Ser. B*, edited by E. K. U. Gross and R. Dreizler (Plenum Press, New York, 1995), .
12. R. van Leeuwen, Phys. Rev. Lett. **80**, 1280 (1998).
13. C. A. Ullrich, U. Gossmann, and E. K. U. Gross, Phys. Rev. Lett. **74**, 872 (1995).
14. J. F. Dobson, M. J. Bünner, and E. K. U. Gross, Phys. Rev. Lett. **79**, 1905 (1997).
15. R. T. Sharp and G. K. Horton, Phys. Rev. **90**, 317 (1953).
16. J. D. Talman and W. F. Shadwick, Phys. Rev. A **14**, 36 (1976).
17. M. Petersilka, U. J. Gossmann, and E. K. U. Gross, in *Electronic Density Functional Theory: Recent Progress and New Directions*, edited by J. F. Dobson, G. Vignale, and M. P. Das (Plenum Press, New York, 1998).
18. T. Grabo, T. Kreibich, S. Kurth, and E. K. U. Gross, in *Strong Coulomb Correlations in Electronic Structure Calculations: Beyond the Local Density Approximation*, edited by V. I. Anisimov (Gordon and Breach, Amsterdam, 2000).
19. J. B. Krieger, Y. Li, and G. J. Iafrate, Phys. Rev. A **45**, 101 (1992).
20. G. Vignale, Phys. Rev. Lett. **74**, 3233 (1995).
21. H. Appel and E. Gross, in *Quantum Simulations of Complex Many-Body Systems: From Theory to Algorithms*, Vol. 10 of *NIC Series*, edited by J. Grotendorst, D. Marx, and A. Muramatsu (John von Neumann Institute for Computing, FZ Jülich, 2002), p. 255.
22. M. Petersilka, U. J. Gossmann, and E. K. U. Gross, Phys. Rev. Lett. **76**, 1212 (1996).
23. D. M. Ceperley and B. J. Alder, Phys. Rev. Lett. **45**, 566 (1980).
24. E. K. U. Gross and W. Kohn, Phys. Rev. Lett. **55**, 2850 (1985).
25. N. Iwamoto and E. K. U. Gross, Phys. Rev. B **35**, 3003 (1987).
26. C.-O. Almbladh and U. von Barth, Phys. Rev. B **31**, 3231 (1985).
27. O. Gunnarsson and B. I. Lundqvist, Phys. Rev. B **13**, 4274 (1976).
28. A. Görling, Phys. Rev. A **47**, 3359 (1999).
29. A. Görling, Phys. Rev. Lett. **85**, 4229 (2000).
30. J. P. Perdew and M. Levy, Phys. Rev. B **31**, 6264 (1985).
31. T. Ziegler, A. Rauk, and E. J. Baerends, Theoret. Chim. Acta **43**, 261 (1977).
32. A. Theophilou, J. Phys. C **12**, 5419 (1979).
33. E. K. U. Gross, L. N. Oliveira, and W. Kohn, Phys. Rev. **A34**, 2805 (1988).

34. E. K. U. Gross, L. N. Oliveira, and W. Kohn, Phys. Rev. **A34**, 2809 (1988).
35. L. N. Oliveira, E. K. U. Gross, and W. Kohn, Phys. Rev. **A34**, 2821 (1988).
36. W. Kohn, Phys. Rev. A **34**, 737 (1986).
37. Á. Nagy, Int. J. Quantum Chem. **69**, 247 (1998).
38. N. I. Gidopoulos, P. G. Papaconstantinou, and E. K. U. Gross, Phys. Rev. Lett. **88**, 033003 (2002).
39. K. Yabana and G. F. Bertsch, Phys. Rev. B **54**, 4484 (1996).
40. E. E. Koch and A. Otto, Chem. Phys. Lett. **12**, 476 (1972).
41. M. A. L. Marques, A. Castro, G. F. Bertsch, and A. Rubio, Computer Phys. Commun. (2002), accepted for publication.
42. A. Zangwill and P. Soven, Phys. Rev. A **21**, 1561 (1980).
43. R. Haensel, G. Keitel, P. Schreiber, and C. Kunz, Phys. Rev. **188**, 1375 (1969).
44. M. P. T. Grabo and E. K. U. Gross, Journal of Molecular Structure (Theochem) **501**, 353 (2000).
45. M. Casida, in *Recent developments and applications in density functional theory*, edited by J. M. Seminario (Elsevier, Amsterdam, 1996), p. 391.
46. C. E. Moore, *Nat. Stand. Ref. Data Ser.* **35** (United States Government Printing Office, Washington, 1971), Vol. I-III.
47. E. S. Nielsen, P. Jørgensen, and J. Oddershede, J. Chem. Phys. **73**, 6238 (1980), erratum: ibid **75**, 499 (1981).
48. E. K. U. Gross, T. Kreibich, M. Lein, and M. Petersilka, in *Electron Correlations and Materials Properties*, edited by A. Gonis, N. Kioussis, and M. Ciftan (Plenum Press, New York, 1999).
49. C. J. Umrigar and X. Gonze, Phys. Rev. A **50**, 3827 (1994).
50. M. A. L. Marques, A. Castro, and A. Rubio, J. Chem. Phys. **115**, 3006 (2001).
51. X. Gonze and M. Scheffler, Phys. Rev. Lett. **82**, 4416 (1999).
52. H. Appel, E. K. U. Gross, and K. Burke, submitted to Phys. Rev. Lett., cond-mat/0203027 (2002).
53. A. Kono and S. Hattori, Phys. Rev. A **29**, 2981 (1984).
54. S. J. A. van Gisbergen *et al.*, Phys. Rev. Lett. **83**, 694 (1999).
55. O. V. Gritsenko and E. J. Baerends, Phys. Rev. A **64**, 042506 (2001).
56. X. Gonze, P. Ghosez, and R. W. Godby, Phys. Rev. Lett. **74**, 4035 (1995).
57. Y.-H. Kim and A. Grling, Phys. Rev. Lett. **89**, 096402 (2002).
58. L. Reining, V. Olevano, A. Rubio, and G. Onida, Phys. Rev. Lett. **88**, 066404 (2002).
59. P. L. de Boeij *et al.*, J. Chem. Phys. **115**, 1995 (2001).
60. G. F. Bertsch, J.-I. Iwata, A. Rubio, and K. Yabana, Phys. Rev. B **62**, 7998 (2000).
61. F. Aryasetiawan, O. Gunnarson, and A. Rubio, Europhys. Lett. **57**, 683 (2002).
62. M. Petersilka, E. K. U. Gross, and K. Burke, Int. J. Quantum Chem. **80**, 534 (2000).
63. Z. Chang *et al.*, Phys. Rev. Lett. **79**, 2967 (1997).
64. C. Spielmann *et al.*, Science **278**, 671 (1997).
65. K. Miyazaki and H. Sakai, J. Phys. B **25**, L83 (1992).
66. C. A. Ullrich, S. Erhard, and E. K. U. Gross, in *Super Intense Laser Atom Physics (SILAP IV)*, edited by H. G. Muller and M. V. Fedorov (Kluwer Publishing Company, Amsterdam, 1996).
67. S. Erhard and E. K. U. Gross, in *Multiphoton Processes*, edited by P. Lambropoulos and H. Walther (IOP Publishing, Bristol, 1996).

68. P. Agostini *et al.*, Phys. Rev. Lett. **42**, 1127 (1979).
69. B. Walker *et al.*, Phys. Rev. Lett. **73**, 1227 (1994).
70. S. Chelkowski and A. D. Bandrauk, J. Phys. B **28**, L723 (1995).
71. M. Petersilka and E. K. U. Gross, Laser Physics **9**, 105 (1999).
72. D. G. Lappas and R. van Leeuwen, J. Phys. B **31**, L249 (1998).